# The Sn isotope composition of chondrites: Implications for volatile element depletion in the Solar System

Xueying Wang, Caroline Fitoussi, Bernard Bourdon, Kevin Righter, Quentin Amet

# The Sn isotope composition of chondrites: implications for volatile element depletion in the Solar System

Xueying Wang[1], Caroline Fitoussi[1], Bernard Bourdon[1], Kevin Righter[2], Quentin Amet[1]

[1]Laboratoire de Géologie de Lyon (LGL-TPE), ENS Lyon, UCBL and CNRS, Université de Lyon, 46 Allée d'Italie, 69364, Lyon Cedex 07, France.

[2]National Aeronautics and Space Administration (NASA) Johnson Space Center, 2101 NASA Parkway, Houston, TX 77058.

Corresponding author: e-mail: bernard.bourdon@ens-lyon.fr

## Abstract

The origin of volatile element depletion in terrestrial planets and meteorites relative to a solar composition represented by CI carbonaceous chondrites remains an unsolved problem. The isotope compositions of moderately volatile elements may offer the possibility to distinguish between the various processes that may have caused this depletion (e.g., partial condensation or partial evaporation). We report high precision Sn isotope measurements in carbonaceous chondrites and ordinary chondrites and the results are reported as $\delta^{124/116}$Sn. Four carbonaceous chondrites (Orgueil CI, Murchison CM2, NWA 5240 CV3 and Allende CV3) show a limited range in $\delta^{124/116}$Sn (-0.02‰ to 0.11‰) with an average value of 0.04±0.11‰ (2 s.d.) for a wide range of Sn concentrations (0.63 ppm to 1.57 ppm). The absence of Sn isotope fractionation among carbonaceous chondrites suggests that volatile depletion may have taken place under thermodynamic equilibrium conditions between solid and vapor in the Solar Nebula. Alternatively, the mixing of two components, a volatile-free component containing no Sn and a volatile-rich component could explain this trend. This latter hypothesis is consistent

with the overall trace element pattern found in carbonaceous chondrites, showing a constant relative abundance when normalized to CI chondrites for the most volatile elements. In contrast with carbonaceous chondrites, ordinary chondrites exhibit a larger range of Sn isotope compositions ($\delta^{124/116}$Sn from-2.02‰ to 0.64‰), but neither the degree of metamorphism (3-6) nor the group (H, L, LL) is correlated with Sn isotopic variations, or with the Sn contents (range 0.20 to 1.44 ppm). Nineteen out of twenty-one ordinary chondrites are enriched in light Sn isotopes compared with carbonaceous chondrites and the bulk silicate Earth. The trace element patterns of volatile elements in ordinary chondrites suggest that equilibrated ordinary chondrites have been disturbed by parent body processes related to metamorphic or shock overprinting but also inherited isotope fractionation found in unequilibrated ordinary chondrites. Last, the isotope composition of the bulk silicate Earth (BSE) indicates that the volatile element depletion observed in the Earth took place in conditions perhaps similar to those of carbonaceous chondrites, as a simple model describing the effect of Earth's core formation on Sn isotopes shows that the Sn isotope composition of the bulk Earth is identical to that of the BSE and of carbonaceous chondrites.

## 1. Introduction

The elemental abundances in CI carbonaceous chondrites (excluding H, C, N, noble gases, Li, B, and partly Be) are similar to the composition of the Sun. In contrast to CI chondrites, other carbonaceous and ordinary chondrites, as well as terrestrial planets show depletions in moderately volatile elements (e.g., Halliday and Porcelli, 2001). These elemental depletions are roughly correlated with volatility as expressed by their condensation temperatures (Wood et al.

2019). Several processes in the early history of the Solar System have been proposed to explain these observations: (i) preexisting volatile element depletion in dust relative to vapor in the Interstellar Medium (Palme and Hutchison, 2001; Yin, 2005), (ii) partial condensation from a hot Solar Nebula (Larimer, 1973; Wasson and Chou, 1974; Grossman and Larimer, 1974; Wai and Wasson, 1977; Cassen, 1996; Cassen, 2001; Albarède, 2009), (iii) partial evaporation during thermal events or due to the migration of volatile-rich material into hotter regions (Alexander, 2005; Ciesla, 2008), (iv) mixing of components with variable volatile element depletion resulting from previous partial vaporization or condensation processes (e.g., Anders, 1964; Larimer and Anders, 1967; Larimer, 1973; Braukmüller et al., 2018; Alexander et al., 2001; Alexander, 2019a), (v) volatile loss during impacts or planetary magmatism (Anders et al., 1976; Larimer and Anders, 1967; Wolf et al., 1980; Hin et al. 2017), (vi) volatile loss during metamorphism (Dodd, 1969; Wasson, 1972; Schaefer and Fegley, 2010). For planetesimals and planets, the incorporation of elements into the core may complicate this picture as many volatile elements are also siderophile or chalcophile. Clearly, the 'volatility trend' showing a decrease in concentrations in the bulk silicate Earth as a function of condensation temperatures (e.g., Palme and O'Neill, 2013) is better constrained for lithophile elements that are not affected by core formation.

It should be mentioned here that process (i) has been dismissed by Palme (2001) as it would introduce heterogeneities in the $^{87}Sr/^{86}Sr$ due to differences in Rb/Sr ratios and these differences have not been found (Palme, 2001). Thus, the preferred hypothesis is that the moderately volatile element depletion is directly linked to early Solar System processes.

In principle, the isotope analysis of moderately volatile elements in meteorites and terrestrial samples could help distinguish between the processes of partial condensation and partial

evaporation. Partial condensation should lead via kinetic effects to light isotope enrichment in the solid, while partial evaporation produces a solid residue enriched in heavy isotopes (Humayun and Cassen, 2000; Davis and Richter, 2013; Bourdon and Fitoussi, 2020). The maximum isotope fractionation should take place in the case of free evaporation in vacuum. However, the isotope fractionation is often limited when evaporation does not take place in vacuum, while elemental depletion is still observed (Young, 2000; Ozawa and Nagahara, 2001; Yu et al., 2003; Davis and Richter, 2013). For example, Humayun and Clayton (1995) and Wang and Jacobsen (2016) had reported no K isotope fractionation in chondrites, achondrites and in the Earth, although K has a clear elemental depletion in terrestrial planets, chondrites and achondrites compared to CI chondrites. A more recent study by Bloom et al. (2020) found variations of K isotopes among chondrites with no clear correlation between K isotope variations and K concentrations. More specifically, evaporation experiments indicated that if the system is in chemical equilibrium, then there is a back-reaction (i.e., condensation) that reduces the kinetic isotope effect of evaporation (e.g., Wombacher et al., 2008; Davis and Richter, 2013). This corresponds to conditions of relatively high partial pressure of the species of interest and in this case the solid can isotopically re-equilibrate with the ambient gas, leading to limited isotope fractionation. Therefore, the elemental fractionation without K isotope fractionation was interpreted as the result of a nearly complete thermodynamic equilibrium caused by the relatively high K partial pressure in the ambient gas (Alexander et al., 2000; Alexander and Grossman, 2005; Fedkin et al., 2006). Altogether, this shows that the isotope fractionation of volatile elements in meteorites and planetary materials can also be a measure of whether a condensed phase was in thermodynamic equilibrium with the vapor phase (Davis and Richter, 2013) .

The measurements of Rb isotopes in chondrites and terrestrial samples reveal small resolvable variations with a total range of a few per mil units (Nebel et al., 2011; Pringle and Moynier, 2017). Notably, there is a positive correlation of $\delta^{87}$Rb with Rb/Sr ratios in carbonaceous chondrites that has been interpreted as a mixture between a volatile-rich component and a volatile-depleted component (Pringle and Moynier, 2017). This interpretation still does not explain the origin of $^{87}$Rb-depleted signature in Rb-depleted chondrites. Similarly, the absence of a $\delta^{87}$Rb difference between Earth and chondrites has been interpreted as reflecting a mixture between 90% of a putative volatile free component (Rb ~ 0 ppm) and 10% of a CI chondrite component (Nebel et al., 2011; Pringle and Moynier, 2017). However, no specific mineral phase or mineral assemblage has been shown to represent this volatile-free component. High precision isotopic measurements of Cd ($T_{50}$ = 652 K by Lodders, 2003, and 502 K by Wood et al., 2019) show that most carbonaceous chondrites including CI, CV, CM, CO and CR have nearly identical Cd isotope compositions (Baker et al., 2010; Wombacher et al., 2008, 2003). In contrast with K and Cd isotopes, Zn isotopes are characterized by decreasing $\delta^{66/64}$Zn values with Zn depletion in carbonaceous chondrites, from CI (average $\delta^{66/64}Zn_{CI}$ = 0.46±0.08‰, 2 s.d.) to CK/CR chondrite ($\delta^{66/64}$Zn = -0.69±0.03‰, 2 s.d.) (Barrat, 2012; Albarède, 2009; Luck et al., 2005; Pringle et al. 2017). This observation was initially interpreted to indicate partial condensation in the early Solar System (Albarède, 2009). Pringle et al. (2017) have attributed this effect to mixing of components involving a volatile-rich component (matrix) and a volatile-poor component that could possibly be chondrules. In addition, the $\delta^{66/64}$Zn value of BSE has been estimated to be 0.28±0.05‰ (2 s.d.) (Chen et al., 2013; Doucet et al., 2016) or 0.16±0.06‰ (Sossi et al., 2018). These values could suggest a role for partial condensation in the solids that accreted to ultimately form the Earth. Similarly, $\delta^{65}$Cu and $\delta^{128/126}$Te for carbonaceous chondrites decreases with increasing volatile element depletion (Luck et al., 2003; Hellmann et

al., 2020). Other studies of volatile elements such as B, Se and Tl have revealed no resolvable variations in planetary materials (Baker et al., 2010; Vollstaedt et al., 2016) and the conclusions of these studies was that elemental depletion was not necessarily coupled with isotope fractionation. In the case of Se, a more recent study (Labidi et al., 2018) has shown variations in Se isotopes among chondrite groups (specifically the EH chondrites) and this was interpreted as a result of kinetic fractionation during sulfidation. In addition, the $\delta^{82/78}$Se of carbonaceous chondrites is correlated negatively with the inverse of Se concentrations (Labidi et al., 2018), similarly to what has been found for Zn and Cu. Overall, based on these studies, there is no simple interpretation regarding the origin of the elemental depletions in meteorites, and while several processes such as free evaporation can be ruled out, the origin of the depletion remains an open question (e.g., Davis, 2006).

Tin is a moderately volatile element with a 50% nebular condensation temperature of 704 K (Lodders, 2003) and recalculated to be 604 K by Wood et al. (2019), which means it would now belong to the category of highly volatile elements. It is depleted in the bulk silicate Earth relative to CI chondrites, by a factor of 33±3 (Jochum et al., 1993). It has ten stable isotopes and is also a potential tracer for investigating the origin of volatile element depletions in planetary materials and the nature of Earth's building blocks. Since Sn is moderately siderophile, its concentration could be affected by core formation, in addition to volatility-driven processes such as condensation and evaporation. The distribution of Sn among different meteorites is poorly known and few direct concentration measurements are available in the literature (e.g., Shima, 1964; Hamaguchi et al., 1969; De Laeter et al., 1974; Braukmüller et al., 2018; Creech and Moynier, 2019). The analysis of the metallic fraction of ordinary chondrites (Shima, 1964) has shown that Sn is enriched in the metal phase by a factor of up to 15, but this enrichment

could be disturbed by thermal metamorphism. Metal-silicate partition coefficients (D) also indicate that Sn is siderophile with a strong dependence on oxygen fugacity, with a D decreasing with increasing pressure (Capobianco et al., 1999; Righter and Drake, 2000; Righter et al., 2010; Righter et al., 2018). Tin can also become chalcophile in the absence of metallic iron. For example, in terrestrial peridotites, Sn is enriched in the minor sulphide phase (Witt-Eickschen et al., 2009). Although Sn isotope compositions of meteorites were analyzed in early studies (e.g., De Laeter and Jeffery, 1967, 1965; Devillers et al., 1983; Loss et al., 1990; McNaughton and Rosman, 1991; Rosman et al., 1984; Rosman and Mcnaughton, 1987), isotope fractionation was not detected outside of the analytical precision (2 s.d. > 0.4‰ using the $\delta^{124/116}$Sn notation). Recent studies of Sn isotopes in terrestrial rocks (Badullovich et al., 2017; Wang et al., 2018) have been used to determine the Sn isotope composition of the bulk silicate Earth. Creech and Moynier (2019) have analyzed a series of chondrites with both ordinary chondrites and enstatite chondrites exhibiting lower $\delta^{124/116}$Sn values than that of the bulk silicate Earth determined by Badullovich et al. (2017). The observed variations were attributed to Sn volatility. These authors concluded that if the Earth was built from enstatite chondrites, this initial Sn isotope signature was removed from the bulk silicate Earth either by volatilization or metal separation. Here, we apply a newly developed MC-ICP-MS technique (Wang et al., 2017) to analyze the Sn isotope composition of carbonaceous and ordinary chondrites to reexamine these questions.

## 2. Samples and analytical methods

A wide variety of chondrites were analyzed in this study as shown in Table 1. Four carbonaceous chondrites, Orgueil (CI), Murchison (CM2), NWA 5240 (CV3) and Allende (CV3) were analyzed for Sn concentrations and Sn isotope compositions. Twenty-one ordinary chondrites with various degrees of metamorphism (Type 3 to 6) belonging to the three groups (H, L, LL) were also analyzed. Among these samples, ten of them belong to the Type 3 chondrites and thus represent unequilibrated ordinary chondrites (UOC) that should have better preserved nebula features, if any.

Diamond disks using for cutting samples often contain bronze that could cause severe Sn contamination. Therefore, to avoid surface contamination, the samples were first crushed into small pieces in an agate mortar and only the internal pieces were carefully selected under optical microscope. The chosen pieces were washed with Milli-Q water in a Teflon beaker. The beaker was then immersed in an ultrasonic bath for 10 min to remove any powder that could originate from the surficial parts of the original sample. The selected pieces were dried under a laminar flow hood. They were then ground to a fine powder in an agate mortar (for the amount of powdered material, see Table S1, Supplementary Material).

The sample dissolution procedure was detailed in our previous study (Wang et al., 2017). Briefly, about 30 mg to 300 mg powdered sample (Table 1) was mixed with $^{117}Sn$-$^{122}Sn$ double spike solution. Then a mixture of 5 mL of concentrated HF and 5 mL of concentrated $HNO_3$ was added and heated on a hot plate at 160 °C for at least 48 hours and subsequently dried down. Then, 4 mL of aqua regia were added to decompose fluorides, after which the solution was dried down and redissolved in 2 mL of concentrated HCl, heated and evaporated twice. Finally, the sample

was dissolved in 1 mL of HCl 0.4 N for further processing. For carbonaceous chondrites, at the end of dissolution process, the samples were taken up in 10 mL of ~1% $H_2O_2$ (this addition does not result in any evaporative loss of Sn as the chemistry yields were ~100%, Wang et al. 2017) and were exposed to UV light for 8 hours to break down organic matter. This treatment efficiently destroys any remaining organic molecules and was shown to stabilize the signal during MC-ICPMS measurements. After the UV treatment, they were evaporated and redissolved in 0.4 M HCl for ion-exchange chromatography.

The purification of Sn was achieved with a three-step ion-chromatography using anion-exchange resin. The protocol, as described in Wang et al. (2017), can separate Sn from the matrix, the elements producing direct isobaric interferences of Sn (i.e., In, Cd and Te) and the elements potentially forming molecular interferences (i.e., Ge, As, Se, Mo and Ag). The overall yield of the chemical separation and purification of Sn was equal to 100±5% (n = 9). Any possible isotope fractionation produced by ion-chromatography and mass spectrometer was corrected with the $^{117}Sn$-$^{122}Sn$ double-spike technique (Wang et al., 2017).

Isotopic measurements of Sn were performed on a multi-collector inductively coupled plasma mass spectrometer (MC-ICP-MS) Neptune Plus (Thermo Scientific), equipped with an Aridus II, Jet sampler cone and X skimmer cone, at the Laboratory of Geology at ENS Lyon. The NIST SRM 3161a standard solution which was purchased from Chemical products for Analysis (CPA) was used as a primary standard. The samples were bracketed by a mixture of NIST SRM 3161a standard with the double spike solution. An in-house secondary standard, which was made from cassiterite ($SnO_2$), was measured repeatedly during a measurement session to check measurement accuracy. The preparation of this secondary standard was described in Wang et

al. (2017). The intensities of Sn isotopes were corrected by an "on-peak zero" technique for each sample to correct molecular isobaric interferences formed from $Ar_3$ (e.g., $^{36}Ar^{40}Ar_2$ and $^{38}Ar_2{}^{40}Ar$ on $^{116}Sn$, $^{38}Ar^{40}Ar_2$ on $^{118}Sn$) as it was shown in Wang et al. (2017) that the level of $Ar_3$ could increase the uncertainties by 30% on the $^{116}Sn/^{122}Sn$ ratio and a factor of ~8 on the $^{120}Sn/^{116}Sn$ ratio. Additionally, $^{116}Sn$ was corrected for the $^{116}Cd$ isobaric interference by monitoring $^{111}Cd$ and assuming a natural $^{111}Cd/^{116}Cd$ ratio. The uncorrected $\delta^{124/116}Sn$ values of our samples are lower and mass-independent when comparing with $\delta^{124/118}Sn$ (see below and Table S2, Supplementary Material), indicating the interference of $^{116}Cd$ on mass 116. The Sn isotope compositions were calculated using a Matlab® program for Sn double-spike inversion based on Rudge et al. (2009). The results are reported as $\delta^{124/116}Sn$ relative to the NIST SRM 3161a standard:

$$\delta^{124/116}Sn = \left(\frac{^{124}Sn/^{116}Sn_{sample}}{^{124}Sn/^{116}Sn_{NIST3161a}} - 1\right) \times 1000 \quad (1)$$

The details of this method, including operating conditions, spike calibration and data reduction are described in Wang et al. (2017). The internal reproducibility on the NIST SRM 3161a standard with a concentration of 10 ppb Sn during a single analytical session is better than ±0.06‰ (2 s.d.) on $\delta^{124/116}Sn$. Repeated Sn isotope measurements of the USGS standard reference andesite AGV-1 from multiple digestions, chemical purification and mass spectrometer measurements yielded a reproducibility of ±0.11‰ on $\delta^{124/116}Sn$ (2 s.d., Wang et al., 2017) during the measurement period of samples reported here. This value is adopted as a realistic external reproducibility for meteorite samples with better apparent reproducibility (i.e., the calculated reproducibility of Allende, based on four independent digestions, is ±0.07‰ but the uncertainty was still reported as ±0.11‰, Table S2, Supplementary Material). The Sn

concentrations of the samples were obtained by an isotope dilution technique using the $^{117}Sn/^{116}Sn$ ratio and the precision is better than 4% (RSD).

## 3. Results

The Sn isotope compositions of twenty-five samples are reported in Table 1 along with Sn contents and plotted in Figure 1. The $\delta^{124/118}Sn$ values were also calculated using $^{118}Sn$, $^{117}Sn$, $^{122}Sn$ and $^{124}Sn$ for the inversion and are listed in Table 1. Figure 2 shows that the $\delta^{124/118}Sn$ versus $\delta^{124/116}Sn$ diagram is characterized by a slope of 0.743±0.040, which is close to the theoretical slope for equilibrium fractionation (0.737) or the kinetic isotope fractionation (0.744). This indicates that isobaric interferences, mass-independent effects including nucleosynthetic isotope anomalies for Sn are smaller than the analytical uncertainties for these samples. A mass-independent fractionation due to variation in nucleus charge radius (Moynier et al. 2009) would affect $^{117}Sn$ (and $^{119}Sn$), thereby disturbing the double-spike inversion and thus fail even the calibration of double-spike (details see Wang et al. 2017), while nucleosynthetic anomalies would affect differently $^{116}Sn$ (s-only process), $^{117}Sn$ $^{118}Sn$ (s- and r-process), $^{122,}$ $^{124}Sn$ (r-only process) (Beer et al., 1989).

The elemental concentrations of Sn for carbonaceous chondrites in this study range from 0.63±0.01 ppm to 1.57±0.13 ppm (2 s.e.). Orgueil (CI) retains the highest concentration among them (1.57±0.13 ppm) and is close to the values of 1.64±0.49 ppm measured by De Laeter et al. (1974), 1.5±0.15 ppm by Friedrich et al. (2002), 1.15±0.06 ppm by Fehr et al. (2005), 1.63±0.3 ppm by Lodders et al. (2009), and 1.55±0.05 ppm by Braukmüller et al. (2018), as well as the compilation value of 1.68±0.17 ppm given by Ebihara et al. (1982) (Table S3, Supplementary Material). Murchison (CM2) contains 0.99±0.08 ppm Sn, also in agreement with literature

247 values of 1.0±0.1 ppm by De Laeter et al. (1974), 0.89±0.09 ppm by Friedrich et al. (2002),
248 0.72±0.2 ppm by Fehr et al. (2005), 0.96±0.05 ppm by Braukmüller et al. (2018), and 0.81±0.27
249 ppm by Creech and Moynier (2019). The average Sn concentration for Allende (CV3) obtained
250 with four individual dissolution replicates is 0.63±0.01 ppm (2 s.e.), also consistent with the
251 values of 0.69±0.27 ppm given by De Laeter et al. (1974), 0.58±0.12 ppm by Friedrich et al.
252 (2003), 0.55±0.05 ppm by Fehr et al. (2005), 0.68±0.01 ppm by Braukmüller et al. (2018), and
253 0.65±0.02 ppm by Creech and Moynier (2019). Another CV3, NWA 5240 contains 1.04±0.08
254 ppm Sn. Carbonaceous chondrites show a limited range of $\delta^{124/116}$Sn values from -0.02±0.11 to
255 0.11±0.11‰ (2 s.d.). According to our analytical uncertainty of ±0.11‰, $\delta^{124/116}$Sn of
256 carbonaceous chondrites are indistinguishable from each other, despite differences in their Sn
257 concentrations. The four meteorites yield a mean $\delta^{124/116}$Sn value for carbonaceous chondrites
258 equal to 0.04±0.11‰.

259 As shown in Table 1, the Sn concentrations of ordinary chondrites vary from 0.20±0.03 to
260 1.44±0.12 ppm and are generally lower than for carbonaceous chondrites (0.63±0.01 to
261 1.57±0.13 ppm). Our Sn concentration range in ordinary chondrites is similar to that reported
262 for L and LL chondrites (Friedrich et al., 2003; Friedrich et al., 2004; Creech and Moynier, 2019,
263 Table S3, Supplementary Material), although there are Sn concentrations as high as 4.7 ppm
264 reported for ordinary chondrites in Friedrich et al. (2003). Ordinary chondrites show a large
265 $\delta^{124/116}$Sn variation from -2.02±0.11 to 0.64±0.11 ‰ (2 s.d.). Compared with carbonaceous
266 chondrites, nineteen out of twenty-one ordinary chondrites have lighter Sn isotope
267 composition than those found for carbonaceous chondrites. The remaining two, Forest Vale (H4)
268 and Dhurmsala (LL6) have $\delta^{124/116}$Sn values that are heavier than carbonaceous chondrites.

Overall, our data set is entirely comparable with the observations reported by Creech and Moynier (2019) for the Sn concentrations. The Sn isotope data is more difficult to compare due to the lack of a common standard. Altogether, Creech and Moynier (2019) reported similar range of variations in $\delta^{124/116}$Sn with strongly negative $\delta^{124/116}$Sn in ordinary chondrites (from -2.16‰ to 1.09‰, calculated based on the reported $\delta^{122/118}$Sn values of the Supplementary Information of Creech and Moynier, 2019) and constant $\delta^{124/116}$Sn for carbonaceous chondrites of CM, C2-ung, CO and CV (from 0.61‰ to 1.23‰ with an average of 0.86‰) identical within error to their value of the bulk silicate Earth (0.98‰). The offset in $\delta^{124/116}$Sn between ordinary chondrites and carbonaceous chondrites is similar to that reported in this study. Creech and Moynier (2019) also measured Sn isotopes in enstatite chondrites and found that their mean $\delta^{124/116}$Sn value is 0.3‰ below that of their BSE. This led them to conclude that if one were to build the Earth from enstatite chondrites, it would require an isotope fractionation between metal/sulfide and silicate during core formation.

## 4. Discussion

### 4.1 Tin isotope signature of carbonaceous chondrites

As shown in Table 1 and Figure 1, the Sn isotope compositions of carbonaceous chondrites (CI, CM and CV) are nearly identical, with an average $\delta^{124/116}$Sn value of 0.04±0.11‰ (2 s.d.). Thus, despite the difference in Sn concentrations in the various carbonaceous chondrite groups, there is no trend in the $\delta^{124/116}$Sn with Sn concentration diagram. These results are consistent with the findings of Creech and Moynier (2019) who also reported constant $\delta^{122/118}$Sn in carbonaceous chondrites. This feature is difficult to explain by the effect of terrestrial alteration, especially since one sample is a find from Northwestern Africa that has been exposed to surface

291 waters. The tin concentrations in surface waters was reported below 0.005 µg/L in a recent
292 study (McVay et al., 2019). Therefore, as there is no systematic Sn isotope differences between
293 the 'falls' and 'finds' of our study, we contend that the Sn isotope signature in chondrites does
294 not reflect the effect of terrestrial weathering. Similarly, the effect of shocks can be dismissed
295 as it would have caused dispersion in the Sn isotopes versus Sn concentration pattern found in
296 carbonaceous chondrites.
297 The effect of aqueous alteration on the parent body of carbonaceous chondrites could in
298 principle have mobilized Sn and modified its isotope composition. One cannot rule out that
299 these effects have taken place, however they do not seem to have modified the $\delta^{124/116}$Sn
300 values in the bulk meteorites.
301 The absence of Sn isotope fractionation, despite variations in Sn contents relative to the bulk
302 Solar System represented by CI chondrites indicates that the Sn depletion recorded in
303 carbonaceous chondrites can be tentatively attributed to an early process in the Solar System.
304 It could be explained from several scenarios: (i) Sn depletion was produced by volatilization
305 under equilibrium conditions or (ii) mixing of a Sn-free component with an Sn-rich matrix
306 similar to the CI chondrites (e.g., Braukmüller et al., 2018; Alexander, 2019a). For the first
307 scenario, as Sn is a siderophile element, its main budget should reside in the metal phase,
308 except in CI chondrites that have no metallic iron. During formation of chondrules at a
309 temperature above 1500 K, it should have rapidly equilibrated with the gas phase, avoiding
310 kinetic isotope fractionation due to evaporation. The magnitude of equilibrium isotope
311 fractionation between Sn metal and SnS vapor can be estimated using the data from Polyakov
312 et al. (2005) and the vibration frequency of SnS in the gas phase (Douglas et al., 1961) to show
313 that the SnS(gas)-Sn(metal) isotope fractionation at 1500 K is 0.04 ‰, suggesting that under

equilibrium conditions the fractionation should be smaller than the observed range in carbonaceous chondrites.

The second scenario assumes that the matrix contains all the Sn and is similar to a CI chondrite composition while another component is Sn-free. This scenario can clearly explain the constant $\delta^{124/116}$Sn in our carbonaceous chondrites. This scenario can be tested simply by plotting the Sn concentration normalized to Si as a function of the fraction of matrix determined in the model of Alexander (2019a). The results are plotted in Figure 3 and show that there is indeed a positive trend suggesting that the fraction of matrix can account for the Sn budget in these meteorites. Importantly, if one calculates the mixing line between the matrix and the volatile-poor component using the Si concentration in the components given in Alexander (2019a), one can show that the mixing line yields a Y-intersection of about 0.02 (Figure 3a). If one simply uses Sn concentrations (Figure 3b), then the trend shows that the matrix-free component could include a significant fraction of Sn. This is consistent with the observations of Hellmann et al. (2020) who showed that, more generally, there was a non-zero abundance in Sn and several other volatile elements in the chondrule component of carbonaceous chondrites. Thus, we consider based on our data that the second model would seem to agree with our observations. It has been found, however, that chondrules in a carbonaceous chondrite (CR) and an L3.05 chondrite did contain Sn at a significant level, suggesting that chondrules are not devoid of volatile elements (Mahan et al., 2018b). However, this may be due to a parent body aqueous alteration. For Allende, Sn-bearing alteration phases have been found in Ca-Al rich inclusions (Ma and Beckett, 2018), indicating Sn mobility towards high temperature components due to aqueous alteration. Thus, it is possible that the Sn concentrations in chondrules may not represent a pristine feature.

337 The nature of the volatile poor component in carbonaceous chondrites was reexamined by
338 Hellmann et al. (2020) who showed that if one uses mass fraction of matrix instead of volume
339 fraction then the moderately volatile element concentrations obtained for the matrix-free
340 endmember, then the concentration of these elements is not equal to zero but that it is
341 remarkably constant when normalized to the CI value. This puzzling information suggests that
342 the chondrule-like fraction is not entirely devoid of these trace elements. If one further
343 assumes that this chondrule-like fraction carries an isotopically fractionated signature, then it
344 can explain the trend between the isotope signature of moderately volatile elements and
345 concentrations (e.g. Luck et al. 2005; Hellmann et al. 2020). Hellmann et al. (2020) further
346 argued that these observations may be reconciled by considering that the chondrule
347 component is itself a mixture of a CI-like component (that dominates the trace element
348 signature) and an isotopically fractionated and more refractory component that would explain
349 the Zn, Cu, K, Te and Rb isotope signatures (Luck et al., 2003; Luck et al., 2005; Pringle et al.,
350 2017; Hellmann et al., 2020; Bloom et al., 2020). In this case, the elements that would be fully
351 condensed would carry no isotope difference with CI chondrites. The isotope fractionation
352 would be seen only in elements that are partly condensed and Te, Zn, Rb, Cu and Cu would fall
353 in this category while Sn, Cd and Tl would be unfractionated.
354 The difficulty in constraining this scenario is that the condensation temperature of elements is
355 only known for canonical conditions (e.g. Wood et al. 2019) but there may be differences or
356 uncertainties owing to variations in the dust/gas ratio during condensation (e.g. Ebel 2000) or
357 uncertainties in the activity coefficients of the elements in the condensates. To illustrate the
358 effect of changing conditions of condensation we have determined the condensation
359 temperatures of the elements of interest for a dust/gas ratio of 1000 (Figure 4) using the
360 activity coefficients given by Wood et al. (2019). This figure illustrates large variations in

condensation temperatures in these conditions compared to the conditions of the Solar Nebula. This shows that it is difficult to know precisely the condensation temperatures of trace elements. Only elements that would be partly condensed would potentially have fractionated isotope signatures. As a toy-model, one could produce the observed isotope patterns in carbonaceous chondrites by considering that the 'chondrule component' consists of one component condensed at high temperature (around 1500 K), while the second component would be formed by condensation around 700 K (Figure 4). In the first high temperature component (dashed line a in Figure 4), one would observe fractionated isotope signatures for Cu, Zn, K (no condensation of Sn, Cd) while the second component (dashed line b in Figure 4) with partial condensation would exhibit fractionation in Rb and Te isotopes (and full condensation of Sn, Cd). This qualitative model is obviously ad-hoc and should be considered as merely illustrative. The chondrule component as defined in Hellmann et al. (2020) would then consist of a CI-chondrite mixed with these higher temperature components in proportions that would match the ~1/10 depletion in moderately elements.

Further constraining such a scenario would require more precise determinations of the condensation temperature in various *T*, *P* and $fO_2$ conditions. One would also need to construct an astrophysical scenario that would justify the presence of components formed at various temperature to make it more realistic.

### 4.2 Sn isotope fractionation in ordinary chondrites

The pattern of volatile element abundances in ordinary chondrites has been interpreted by partial condensation from the Solar Nebula (Ikramuddin et al., 1977; Wai and Wasson, 1977;

383 Morgan et al., 1985), by mixing and fractionation of various components (Alexander, 2019b), by
384 metamorphism on the parent body (e.g., Schaefer and Fegley, 2010) or by shock volatility (e.g.,
385 Friedrich et al., 2004). Similarly, there has been competing interpretations of the isotope
386 signature of volatile elements in ordinary chondrites. For example, Zn isotope variations in
387 ordinary chondrites were interpreted as due to condensation of a vapor enriched in light
388 isotopes (Luck et al., 2005), while Wombacher et al. (2008) argued that the Zn-Cd trace element
389 patterns combined with the Cd isotope indicated open-system parent body metamorphism.
390 The disturbed positive trend between Zn versus Sn concentrations (Figure 5) is consistent with
391 the observations made for Cd-Zn and suggests that Sn has also been affected by secondary
392 processes rather than being solely controlled by volatility (in which case it should show a well-
393 defined positive correlation). In contrast, Pringle et al. (2017) interpreted the light Zn isotopic
394 compositions of ordinary chondrites being due to the loss of a Zn-bearing sulphide in the
395 nebula. The stable Te and Ag isotope record of ordinary chondrites has also been interpreted
396 as the result of multiple stages of metamorphism involving both evaporation and condensation
397 (Schönbächler et al., 2008; Fehr et al., 2018). Interestingly, the complex processes that were
398 invoked for explaining the Zn isotope record of ordinary chondrites did not cause any Se
399 isotope fractionation according to the study of (Vollstaedt et al., 2016), while a more recent
400 study by Labidi et al. (2018) suggests a correlation between $\delta^{82/78}$Se and Se concentrations in
401 carbonaceous chondrites.
402
403 Overall, the Sn isotope signature observed in ordinary chondrites is similar to that of other
404 moderately volatile elements. First, the Sn concentration in ordinary chondrites (Figure 5)
405 shows a similar pattern to that of Ag (Schönbächler et al., 2008) and Cd (Wombacher et al.,
406 2008) which are both very scattered suggesting the importance of secondary processes. Second,

the observation of both enrichment and depletion in light Sn isotopes relative to the CI chondrite composition indicates the interplay of at least two processes (e.g., evaporation + condensation) rather than a single process (e.g., evaporation only). Last, the significant range in $\delta^{124/116}$Sn found in unequilibrated ordinary chondrites (-2.02 to -0.19‰) suggests that nebular processes must have played a role in the observed variations. For volatile elements, we do not necessarily expect that their stable isotope record should be homogenized prior to accretion and this is what we observe, which is L and LL chondrites that do not have identical $\delta^{124/116}$Sn values in Types 3.0-3.2 samples (Table 1). Furthermore, the mean $\delta^{124/116}$Sn value for unequilibrated ordinary chondrites is -0.71±0.27‰ (2 s.e.), which is resolvably below the mean value obtained for carbonaceous chondrites (0.040±0.054‰, 2 s.e.), as confirmed by a statistical t-test. This means that ordinary chondrites indicate that a nebular event produced an Sn isotope fractionation relative to the Solar composition. Such an offset could in principle be explained by a kinetic isotope effect during partial condensation (Figure 6), rather than equilibrium fractionation that should be more subdued.

It was hypothesized by Larimer (1973) and Wasson and Chou (1974) that the variations in metallic iron abundances found among the ordinary chondrites was due to partial loss of metallic Fe during an early stage of the protoplanetary disk (e.g., Pignatale et al., 2019). Since the budget of siderophile elements is dominated by the metallic phase, the partial separation of metal should deplete these elements in the resulting bulk L and LL chondrites. It turns out that this is the case for the most refractory elements down to Ge (Larimer 1973) whose condensation temperature is 883 K given by (Lodders, 2003) and 830 K by Wood et al. (2019). For the more volatile elements such as Sn, there is no observed difference among the three ordinary chondrite groups, suggesting that elements more volatile than Ge (including Sn)

condensed in the remaining metal after this fractionation event. The absence of variations in Sn concentrations for the various types of ordinary chondrites (Figure 7, Figure 8) would indeed suggest that the Sn budget was not controlled by the variable amount of metal present in ordinary chondrites. Therefore, the separation of metal itself cannot explain the Sn isotope fractionation in ordinary chondrites and this isotope fractionation by condensation would have taken place once the metal was separated from silicate.

Although ordinary chondrites may carry a nebular signature in Sn isotopes, there is also a clear signature of parent body processes. In the context of metamorphism, Sn is not the most mobile element compared with other volatile elements (Schaefer and Fegley, 2010). The data compilation of Schaefer and Fegley (2010) shows that Sn does not exhibit greater depletion from Type 3 to Type 6 chondrites, although there is clearly a lack of data compared with other elements. The calculated sequence of volatility at 1 bar calculated by Schaefer and Fegley (2010) would place Sn between Se and Tl. Selenium shows similar concentrations for Type 3 to Type 6, while a marked depletion is observed for Tl (Schaefer and Fegley, 2010). A limitation of this calculation is that the 'formation temperature' for volatile elements at 1 bar are 2300, 2302 and 2225 K for Sn, Se and Tl, respectively, in ideal solid solutions, which are well above the temperatures experienced by ordinary chondrites during metamorphism. These thermodynamic calculations are, therefore, more useful to evaluate relative volatility than to estimate the absolute temperatures at which these elements were mobilized. Note that the chosen pressure is at the low end of pressures inside a 100 km planetesimal, given that the permeabilities of chondrites determined in Bland et al. (2009) is in the $10^{-17}$ $m^2$ range indicating slow gas flow at the scale of a planetesimal (Sugiura et al. 1984). This indicates that gas pressure should be controlled by the lithostatic pressure.

453 In investigating the mobility of Sn in ordinary chondrites, an important question is to identify
454 the primary mineral hosts of Sn. In principle, most of the Sn should be contained in the metal
455 fraction and this is confirmed by a few analyses that reported Sn concentrations for metal and
456 silicate separates (Hamaguchi et al. 1969; Mason and Graham 1970). The analysis of Shima
457 (1964) showed a greater Sn concentration in the metal fraction by at least a factor of 10. For
458 the oxygen fugacities calculated in ordinary chondrites (Grossman et al. 2008), there should
459 indeed be a predominance of Sn as Sn(0) in the metal fraction with a small amount as Sn(II) in
460 the silicates. There should be by comparison less Sn stored in sulfides (e.g., van Acken et al.,
461 2012). Upon metamorphism, it has been suggested that Type 3 chondrites could have first been
462 oxidized due to the release of water and then reduced due to the presence of graphite and
463 organic matter (Huss et al., 2006), while Type 4 to 6 would have been oxidized (McSween and
464 Labotka, 1993), as water is released from phyllosilicates, which explains the positive correlation
465 between $\Delta^{17}O$ and fayalite content in olivine in ordinary chondrites (Rubin, 2005). The
466 associated oxidation in types 4-6 could have caused a redistribution of Sn into silicate phases by
467 reducing the metal/silicate partition coefficient.
468
469 In order to reevaluate whether Sn could be mobilized during parent body processes, we have
470 modelled the thermodynamic conditions during metamorphism between 200 K and 1200 K to
471 evaluate whether a significant amount of Sn could be mobilized in a gas phase containing water
472 that could oxidize Fe and release siderophile elements such as Sn or aqueous phase using the
473 FACTSAGE™ software (Bale et al., 2009; Bale et al., 2016). We have not attempted to model
474 precisely the distribution of Sn in the silicate due to a lack of partitioning data. The FACTSAGE
475 software includes a large data base of solid solutions data for iron-dominated metals (FT-Stel)
476 that is particularly relevant for studying Sn that partitions into the iron metal at the relevant

oxygen fugacities. In order to model this system, we have used the chemical compositions of H and L chondrites reported in Wasson and Kallemeyn (1988) for the following elements (H, C, O, Na, Mg, Al, Si, S, Cl, Ca, Fe, Ni, Sn). Overall, there can be a sizeable amount of Sn in the gas phase for temperature above 600-650 K. The main species in the vapor phase is $SnCl_2$ for temperatures ranging between 750 K and 1200 K (Figure 9) at a pressure of 1 bar. This means that there should be little Sn loss for the Type 3.1-3.3, while Sn loss could have taken place for Types greater than 3.4 (see compilation of metamorphic temperatures by Huss et al. 2006). Thus, it becomes clear with these simulations that the abundance of chlorine in ordinary chondrites (11-400 ppm in type 3-4; Sharp et al. 2013; Clay et al. 2017) is sufficient to allow partitioning of Sn in the gas phase at relatively low temperatures. It has been suggested by McSween and Labotka (1993) and Rubin (2005) that metamorphism was accompanied by oxidation and this was due to hydrous fluids. Thus, we also investigated the mobility of Sn in a putative water phase. However, our thermodynamic calculations show that there was little Sn in the aqueous phase. One may note also that the L chondrite parent body was presumably affected by a cataclysmic event but since Sn isotopes in L chondrites seem rather similar to those of H and LL chondrites and the $\delta^{124/116}$Sn is not correlated with shock level in L chondrites, it is hard to call upon a specific effect on Sn isotopes in the L chondrite group.

The exact effect of releasing $SnCl_2$ during metamorphism of ordinary chondrites (500-850 K) on the Sn isotope signature is more difficult to assess. In principle, if the diffusion of Sn in the rock to the porous space and the migration of $SnCl_2$ in the gas phase is associated with kinetic isotope fractionation, then the $SnCl_2$ species should be enriched in light Sn isotopes, while the solid residue should be enriched in heavy Sn isotopes. If this gas phase is later trapped in the solid, then the solid should be enriched in light isotopes while getting enriched in Sn with an

501 effect depending on the initial Sn budget of the solid. If one assumes that the initial $\delta^{124/116}$Sn
502 and Sn concentrations are equal to that of Type 3 ordinary chondrites, this process would lead
503 to a negative trend in the $\delta^{124/116}$Sn versus Sn concentration diagram, which does not
504 correspond to the observed pattern (Figure 8). On the other hand, it is possible that the release
505 of $SnCl_2$ took place with equilibrium isotope fractionation rather than kinetic isotope
506 fractionation. In this case, one predicts that at 700 K, the $SnCl_2$ species should be enriched in
507 heavy isotopes rather than light isotopes (Wang et al., 2019). Thus, the condensation of Sn-rich
508 vapor would result in an enrichment in Sn and in heavy Sn isotopes, a process that may explain
509 the enrichment in heavy Sn isotopes in our samples of Dhurmsala (LL6) and Forest Vale (H4).
510 While this scenario is difficult to verify with the existing data, it has the merit of being more
511 compatible with the observations.
512 Overall, our Sn isotope observations for ordinary chondrites are consistent with previous
513 volatile element data and suggests that superposition of nebular processes and parent body
514 metamorphism could explain the $\delta^{124/116}$Sn variations. It is clear that a more detailed
515 description of the proposed scenario would require an investigation of Sn isotope systematics
516 at the mineral scale, which is still beyond current analytical capabilities due to low Sn
517 concentrations.
518

519 **4.3 A Sn isotope signature of volatile element depletion in the Earth**

520 The depletion in moderately volatile elements in the Earth is not fully understood. Similarly to
521 chondrites, its Sn isotope composition may be an indicator of the process of volatile element
522 depletion. Early work had suggested, based on the moderately volatile element pattern as a
523 function of condensation temperatures that the Earth was built from two components, a

524 volatile-free component and a volatile-rich component similar to CI chondrites (Anders et al.,
525 1977). This approach was reemphasized by later work defining the model of 'heterogeneous
526 accretion' for the Earth (Wanke and Dreibus, 1988; O'Neill, 1991). More recently, Schönbächler
527 et al. (2010) have shown that a heterogeneous accretion could account for the Pd-Ag
528 systematics of the Earth and chondrites. Based on modeling nucleosynthetic anomalies and O
529 isotopes, Fitoussi et al. (2016) showed that the Earth could be built by a mixture of angrites, H,
530 CI, and CV chondrites that are heterogeneous in their volatile element contents with an overall
531 CI + CV chondrite contribution of 18%, while Dauphas (2017) argued that the Earth was mainly
532 built from an enstatite-like reservoir. More recently, Budde et al. (2019) showed that the last
533 10-20% of accretion required a carbonaceous chondrite component to explain the Mo isotopes
534 in the bulk silicate Earth.

535 The Sn isotope composition of the bulk silicate Earth is identical to that of carbonaceous
536 chondrites. However, as Sn is a siderophile element, most of the Sn budget should reside in the
537 core rather than the silicate Earth. In order to assess the Sn isotope composition of the bulk
538 Earth, one must first determine the effect of core formation on the Sn isotope composition. In
539 principle, Sn is considered as a moderately siderophile element with an estimated bulk
540 metal/silicate partition coefficient close to ~10 for the conditions of terrestrial core formation
541 (Righter et al., 2018). This suggests that the Sn isotope composition of BSE could potentially be
542 affected by core formation and this effect must first be assessed before focusing on the Sn
543 depletion in the bulk Earth. We established a simple model for Sn isotopic fractionation during
544 Earth's core formation as a function of various parameters (*P*, *T*, the oxygen fugacity $fO_2$, etc.)
545 using the metal-silicate partition coefficient defined in the Supplementary Material. Then,
546 following Righter et al. (2017), we have used the liquidus for mantle melting of Andrault et al.

(2011) which is a function of pressure and two different cases: a fixed $fO_2$ at IW-2 or a variable $fO_2$ ranging between IW-4 and IW-1.6 over the considered temperature range (2000-4000 K). The oxygen fugacity increases incrementally with accretion as described in Righter et al. (2017). Figure 10 shows the calculated partition coefficient of Sn between metal and silicate ($D_{Sn}$) as a function of temperature corresponding to the two evolution models. It demonstrates that with fixed $fO_2$, $D_{Sn}$ is almost constant, while with variable $fO_2$ between IW-4 and IW-1.6, $D_{Sn}$ decreases with increasing temperature and pressure.

Altogether, the difference of the Sn isotope compositions between the BSE and the bulk Earth expressed as $\Delta^{124}Sn_{BSE-Bulk\ Earth}$, can be calculated by the following equation (see Supplementary Material for derivation):

$$\Delta^{124/116}Sn_{BSE-Bulk\ Earth} = \left[\frac{D_{Sn}X_{core}}{D_{Sn}X_{core}+1-X_{core}}\right] \times \mathrm{A} \times T^{-2} \quad (2)$$

where $X_{core}$ is the mass fraction of core in the bulk planet. A is a constant equal to $0.32 \times 10^6$ for SnO-Sn system and $0.776 \times 10^6$ for $SnO_2$-Sn system, respectively. Since $D_{Sn}$ can be expressed as a function of temperature (see Supplementary Material), it is possible to express $\Delta^{124/116}Sn_{BSE-Bulk\ Earth}$ as a function of temperature. The results of model calculations predicting $\Delta^{124/116}Sn_{BSE-Bulk\ Earth}$ as a function of temperature are plotted in Figure 11 for various evolutions of $fO_2$ during core formation. The deeper *P-T* conditions where metal and silicate equilibrated during core formation in the Earth are estimated to be higher than 3000 K and up to 3800 K (Righter 2011; Siebert et al., 2011; Fischer et al., 2015), associated with a maximum $\Delta^{124}Sn_{BSE-Bulk\ Earth}$ value of 0.005 ‰ (for Sn(II)-Sn(0) fractionation) and 0.05 ‰ for Sn(IV)-Sn(0) fractionation (Figure 11), which is much smaller than the currently achieved precision of $\delta^{124/116}$Sn measurements (±0.11 ‰, 2 s.d.).

569 Therefore, the effect of core formation on Sn isotopes can be neglected in the case of the
570 Earth. The Sn isotope composition of BSE is predicted to be identical, within error, to that of
571 the bulk Earth, with a $\delta^{124/116}$Sn value of -0.08±0.11‰ (2 s.d.) as determined in Wang et al.
572 (2018). This difference is comparable with the results obtained by Badullovich et al. (2017)
573 and Creech and Moynier (2019), although the absence of a common standard in the two sets
574 of studies makes a strict comparison difficult. As a result, the $\delta^{124/116}$Sn value of the bulk
575 Earth is identical to that of carbonaceous chondrites. However, Cr nucleosynthetic anomalies
576 found in the Earth are not identical to those of carbonaceous chondrites (Trinquier et al.,
577 2007), indicating that the Earth is not predominantly built from carbonaceous chondrites.
578 Our modeling also disagrees with the interpretations of Creech and Moynier (2019) who
579 argued that an enstatite chondrite-like Earth could explain the observed BSE composition
580 due to the effect of core formation. The nature of the Earth's building blocks is a topic of
581 discussion (Dauphas 2017; Fitoussi et al., 2016) and the stable isotope composition of
582 building blocks could have been affected by early processes such as those described for
583 chondrites or by large impacts or magma ocean volatilization (Hin et al., 2017; Pringle et al.,
584 2014). However, in the context of a model where volatile elements were accreted to the
585 Earth by carbonaceous chondrite like material (e.g., Fitoussi et al. 2016), it is possible that an
586 early magma ocean had operated and produced a proto-Earth with an isotopically
587 fractionated Sn signature. However, the budget of Sn was subsequently overwhelmed by Sn-
588 rich material identical to that of carbonaceous chondrites. If one were to argue that the Earth
589 had acquired its volatile budget from ordinary chondrites, there should be a process able to
590 raise the $\delta^{124}$Sn of these chondrites (mean $\delta^{124}$Sn value = -0.707±0.27‰ 2 s.e.) to the BSE
591 value. One would have to call upon a large-scale evaporation such as a magma ocean that
592 would have fortuitously raised the $\delta^{124}$Sn to a value identical to that of carbonaceous

chondrites and of the BSE. In addition, there is no signature of partial condensation (Albarède, 2009) or removal of a sulfide component (Pringle et al., 2017) as has been argued for Zn isotopes. If the Earth's budget in moderately volatile elements is due to the addition of a volatile rich component, then this component must have had an Sn isotope signature similar to carbonaceous chondrites (as seen with other isotope systems, e.g., Wombacher et al., 2008).

## 5. Conclusions

The Sn isotope compositions of four carbonaceous chondrites including Orgueil CI, Murchison CM, NWA 5240 CV and Allende CV have been analyzed and exhibit $\delta^{124/116}$Sn values within a limited range (average 0.04±0.11‰, 2 s.d.) which is comparable to that of BSE (-0.08±0.11‰, 2 s.d., Wang et al., 2018). This result indicates that the Sn depletion in carbonaceous chondrites cannot be used to discriminate partial evaporation from partial condensation in the early Solar Nebula. Instead, it suggests that Sn isotope fractionation was limited and this could be due to thermodynamic equilibrium conditions between condensed phase and the ambient vapor in the early Solar Nebula. However, in light of other observations, the Sn isotope data is more consistent with a model involving the mixing of a refractory component (depleted in Sn) with a CI-like component volatile rich component. This model would agree with the general volatile element pattern in carbonaceous chondrites.

The Sn isotope record in carbonaceous chondrites is consistent with other volatile elements that have constant relative abundances and are linked to the abundance of a matrix-like component. In contrast, other less volatile elements such as K, Rb and Cu (and possibly also Zn)

615 show an isotope fractionation pattern indicating that part of their budget is contained in the
616 refractory component of carbonaceous chondrites. A better knowledge of the condensation
617 temperature of moderately volatile element would be desirable to fully understand their
618 isotope signatures.

619 By comparison, ordinary chondrites show greater variations in Sn isotope compositions and are
620 most often enriched in light Sn isotopes compared with carbonaceous chondrites. The $\delta^{124/116}$Sn
621 values of ordinary chondrites show no correlation with degrees of metamorphism (Type 3 to 6)
622 or groups (H, L, LL) but the overall dispersion in $\delta^{124/116}$Sn could be explained by volatilization of
623 $SnCl_2$ during metamorphism. The enrichment in light Sn isotopes found in unequilibrated
624 ordinary chondrites could be the consequence of partial condensation of Sn due to a kinetic
625 isotope effect but the details of such a process would require mineral scale analysis of Sn
626 isotopes. Last, our modeling shows that the Sn isotope composition of the bulk Earth should be
627 identical to that of the bulk silicate Earth and to that of carbonaceous chondrites, because of
628 the limited fractionation effect expected from core formation.

629

630 **Acknowledgements**

631 We gratefully acknowledge ANR project ISOVOL (ANR-12-BS06-0002-01), LABEX LIO (ANR-10-
632 LABX-0066) and ERC COSMOKEMS project (# 694819) for financial support. We thank Philippe
633 Telouk for maintaining the Neptune plus in good operation. We thank Conel Alexander and
634 anonymous reviewers and the associated editors, Munir Humayun and Thorstein Kleine for
635 providing constructive and insightful comments that helped improve the manuscript.

636

637 **Figure captions**

638 Figure 1 $\delta^{124/116}$Sn analyzed by MC-ICPMS using double-spike technique. $\delta^{124/116}$Sn of BSE is
639 from Wang et al. (2018). All the uncertainties better than AGV-1 (0.11‰ for 2 s.d.) are reported
640 as 0.11‰.
641
642 Figure 2 $\delta^{124/116}$Sn versus $\delta^{124/118}$Sn as listed in Table 1, with a slope of 0.743±0.04. All the
643 uncertainties better than AGV-1 are given as 0.11‰ (2 s.d.) on $\delta^{124/116}$Sn and 0.10‰ (2 s.d.) on
644 $\delta^{124/118}$Sn.
645
646 Figure 3 (a) Sn/Si normalized to CI chondrites versus mass fraction of matrix in % for
647 carbonaceous chondrites and Tagish Lake meteorite (TL). Sn and Si concentrations are from
648 Alexander (2019a) except for Sn concentrations for CI and CV chondrites which are from this
649 study. (b) Sn concentrations versus mass fraction of matrix in % for carbonaceous chondrites
650 and Tagish Lake meteorite (TL). The Y-intersect is not equal to zero, indicating the presence of
651 Sn in the chondrule component.
652
653 Figure 4 Condensation curves for a selection of moderately volatile elements using the
654 FACTSAGE™ software with a solar composition from Lodders (2003) with a dust enrichment
655 factor of 1000 and P = $10^{-3}$ atm. Activity coefficients for trace elements were taken from Wood
656 et al. (2019). Note the significant shift in the condensation temperature of Zn and Te relative to
657 Sn that is consistent with the difference in their isotopic signatures. The dashed line (a) show
658 the condensation temperature necessary to obtain isotope fractionation in Zn, Cu and K, while
659 line (b) corresponds to the condensation temperature for isotope fractionation of Te and Rb. Cd
660 and Sn should show no fractionation in both cases.
661
662 Figure 5 Compilation of Sn concentrations versus Zn concentrations in chondrites. Data source
663 are: Wasson and Kallemeyn (1988) for the carbonaceous chondrites, Friedrich et al. (2003),
664 Friedrich et al. (2004), Friedrich et al. (2014) for the L and LL chondrites and Creech and
665 Moynier (2019).
666
667

Figure 6 Diagram illustrating the effect of (a) partial condensation and (b) partial evaporation using a Rayleigh distillation in a $\delta^{66/64}$Zn versus Zn normalized to the Zn concentration in CI. The $\delta^{66/64}$Zn values are given relative to the value for CI chondrite from Luck et al. (2005). Zn isotope data are from Luck et al. (2005) and Mahan et al. (2018a). The various curves are calculated as a function of $P_{i\ sat}/P_i$ (ratio of saturation pressure to the partial pressure of the isotope of interest i) for diagram (a) and $P_i/P_{i\ sat}$ for diagram (b) with the model of Dauphas et al. (2015) for the global isotope fractionation factor. Three conditions were calculated using $P_{i\ sat}/P_i$ = 0.9, 0.95 and 1 for diagram (a) and $P_i/P_{i\ sat}$ = 0.95, 0.98 and 1 for diagram (b), respectively. The kinetic isotope fractionation factor is equal to $\sqrt{64/66}$. The equilibrium isotope fractionation factor was taken from Ducher et al. (2016) corresponding to an equilibrium between ZnO(solid) and Zn(gas).

Figure 7 Histograms of Sn concentrations in H chondrites, L chondrites, and LL chondrites. Data source are Friedrich et al. (2003), Friedrich et al. (2004), Friedrich et al. (2014) for the L and LL chondrites and Creech and Moynier (2019) and this study. The data shows no difference between the three ordinary chondrite groups.

Figure 8 $\delta^{124/116}$Sn versus Sn concentrations in ordinary chondrites (data from Table 1). The unequilibrated chondrites are marked with a black circling. The only positive $\delta^{124/116}$Sn are found for equilibrated chondrites.

Figure 9 Sn volatility in ordinary chondrites calculated at 1 atm. The Sn speciation was calculated for an H chondrite bulk composition and the main volatile species is $SnCl_2$. The other species are $SnCl_4$ or SnS but are too low to be shown in this diagram. FCC and BCC indicates two allotropes of the iron alloy. The calculations were made for three Cl concentrations: 11 ppm, 80 ppm, 400 ppm corresponding to the minimum, the mean and the maximum concentrations, respectively. The minimum and the maximum Cl concentrations are from the literature (Sharp et al. 2013; Clay et al. 2017).

Figure 10 (a) Calculated metal-silicate partition coefficient for tin as a function of temperature (in K) and pressure corresponding to the mantle melting curve of Andrault et al. (2011) (after Righter et al., 2017). The model curves were calculated for two evolution models. The fixed $fO_2$

cases correspond to IW-2, while the variable $fO_2$ values range from IW-4 to IW-1.6, as might be expected during a heterogeneous accretion scenario. The light green boxes illustrate the temperature of the magma ocean.

Figure 11 Calculated difference of $\delta^{124/116}$Sn between the BSE and the bulk Earth expressed as $\Delta^{124/116}Sn_{BSE-Bulk\ Earth}$ as a function of temperature corresponding to the two $fO_2$ evolution models. (a): model curves calculated assuming Sn(IV) is the dominant species in the silicate melt, (b) : model curves calculated assuming Sn(II) is the dominant species in the silicate melt. In both cases, $\Delta^{124/116}Sn_{BSE-Bulk\ Earth}$ at temperatures > 3000 K is below our measurement precision of 0.11 ‰ (2 s.d.).

**References**


van Acken D., Humayun M., Brandon A. D. and Peslier A. H. (2012) Siderophile trace elements in metals and sulfides in enstatite achondrites record planetary differentiation in an enstatite chondritic parent body. *Geochim. Cosmochim. Acta* **83**, 272–291.

Albarède F. (2009) Volatile accretion history of the terrestrial planets and dynamic implications. *Nature* **461**, 1227–1233.

Alexander C. M. O. D. (2019a) Quantitative models for the elemental and isotopic fractionations in chondrites: The carbonaceous chondrites. *Geochim. Cosmochim. Acta* **254**, 277–309.

Alexander C. M. O. D. (2019b) Quantitative models for the elemental and isotopic fractionations in the chondrites: The non-carbonaceous chondrites. *Geochim. Cosmochim. Acta* **254**, 246–276.

Alexander C. M. O. D. (2005) Re-examining the role of chondrules in producing the elemental

726 fractionations in chondrites. *Meteorit. Planet. Sci.* **40**, 943–965.
727 Alexander C. M. O. D., Boss A. P. and Carlson R. W. (2001) The early evolution of the inner solar
728 system: A meteoritic perspective. Science **293**, 64-68.
729 Alexander C. M. O. D. and Grossman J. N. (2005) Alkali elemental and potassium isotopic
730 compositions of Semarkona chondrules. *Meteorit. Planet. Sci.* **40**, 551–556.
731 Alexander C. M. O., Grossman J. N., Wang J., Zanda B., Bourot-Denise M. and Hewins R. H.
732 (2000) The lack of potassium-isotopic fractionation in Bishunpur chondrules. *Meteorit.*
733 *Planet. Sci.* **35**, 859–868.
734 Anders E. (1964) Origin, age and composition of meteorites. Space Sci. Rev. 3, 583-714.
735 Anders E., Higuchi H., Ganapathy R. and Morgan J. W. (1976) Chemical fractionations in
736 meteorites-IX. C3 chondrites. *Geochim. Cosmochim. Acta* **40**, 1131–1139.
737 Anders E., Massey H. S. W., Brown G. M., Eglinton G., Runcorn S. K. and Urey H. C. (1977)
738 Chemical compositions of the Moon, Earth, and eucrite parent body. *Philos. Trans. R. Soc.*
739 *London. Ser. A, Math. Phys. Sci.* **285**, 23–40.
740 Andrault D., Bolfan-Casanova N., Nigro G. Lo, Bouhifd M. A., Garbarino G. and Mezouar M.
741 (2011) Solidus and liquidus profiles of chondritic mantle: Implication for melting of the
742 Earth across its history. *Earth Planet. Sci. Lett.* **304**, 251–259.
743 Badullovich N., Moynier F., Creech J., Teng F. Z. and Sossi P. A. (2017) Tin isotopic fractionation
744 during igneous differentiation and Earth's mantle composition. *Geochemical Perspect. Lett.*
745 **5**, 24–28.
746 Baker R. G. A., Schönbächler M., Rehkämper M., Williams H. M. and Halliday A. N. (2010) The
747 thallium isotope composition of carbonaceous chondrites - New evidence for live 205Pb in
748 the early solar system. *Earth Planet. Sci. Lett.* **291**, 39–47.
749 Bale C. W., Bélisle E., Chartrand P., Decterov S. A., Eriksson G., Gheribi A. E., Hack K., Jung I. H.,
750 Kang Y. B., Melançon J., Pelton A. D., Petersen S., Robelin C., Sangster J., Spencer P. and
751 Van Ende M. A. (2016) FactSage thermochemical software and databases, 2010-2016.
752 *Calphad Comput. Coupling Phase Diagrams Thermochem.* **54**, 35–53.
753 Bale C. W., Bélisle E., Chartrand P., Decterov S. A., Eriksson G., Hack K., Jung I. H., Kang Y. B.,
754 Melançon J., Pelton A. D., Robelin C. and Petersen S. (2009) FactSage thermochemical
755 software and databases - recent developments. *Calphad Comput. Coupling Phase*
756 *Diagrams Thermochem.* **33**, 295–311.
757 Barrat J. A., Zanda B., Moynier F., Bollinger C., Liorzou C., Bayon G. (2012) Geochemistry of CI

chondrites: Major and trace elements, and Cu and Zn isotopes. *Geochim. Cosmochim. Acta* **83**, 79-92.

Beer H., Walter G., Kappler F., Beer H., Walter G. and Kappler F. (1989) *S-process studies on tin*.,

Bland P. A., Jackson M. D., Coker R. F., Cohen B. A., Webber J. B. W., Lee M. R., Duffy C. M., Chater R. J., Ardakani M. G., McPhail D. S., McComb D. W. and Benedix G. K. (2009) Why aqueous alteration in asteroids was isochemical: High porosity ≠ high permeability. *Earth Planet. Sci. Lett.* **287**, 559–568.

Bloom H., Lodders K., Chen H., Zhao C., Tian Z., Koefoed P., Pető M. K., Jiang Y. and Wang (王昆) K. (2020) Potassium isotope compositions of carbonaceous and ordinary chondrites: Implications on the origin of volatile depletion in the early solar system. *Geochim. Cosmochim. Acta* **277**, 111–131.

Bourdon B. and Fitoussi C. (2020) Isotope Fractionation during Condensation and Evaporation during Planet Formation Processes. *ACS Earth Sp. Chem.* **4**, 1408–1423.

Braukmüller N., Wombacher F., Hezel D. C., Escoube R. and Münker C. (2018) The chemical composition of carbonaceous chondrites: Implications for volatile element depletion, complementarity and alteration. *Geochim. Cosmochim. Acta* **239**, 17–48.

Budde G., Burkhardt C. and Kleine T. (2019) Molybdenum isotopic evidence for the late accretion of outer Solar System material to Earth. *Nature* **3**, 736–741.

Capobianco C. J., Drake M. J. and De'Aro J. (1999) Siderophile geochemistry of Ga, Ge, and Sn: Cationic oxidation states in silicate melts and the effect of composition in iron-nickel alloys. *Geochim. Cosmochim. Acta* **63**, 2667–2677.

Cassen P. (1996) Models for the fractionation of moderately volatile elements in the solar nebula. *Meteorit. Planet. Sci.* **31**, 793–806.

Cassen P. (2001) Nebular thermal evolution and the properties of primitive planetary materials. *Meteorit. Planet. Sci.* **36**, 671–700.

Chen H., Savage P. S., Teng F. Z., Helz R. T. and Moynier F. (2013) Zinc isotope fractionation during magmatic differentiation and the isotopic composition of the bulk Earth. *Earth Planet. Sci. Lett.* **369**–**370**, 34–42.

Ciesla F. J. (2008) Radial transport in the solar nebula: Implications for moderately volatile element depletions in chondritic meteorites. *Meteorit. Planet. Sci.* **43**, 639–655.

Clay P. L., Burgess R., Busemann H., Ruzié-Hamilton L., Joachim B., Day J. M. D. and Ballentine C. J. (2017) Halogens in chondritic meteorites and terrestrial accretion. *Nature* **551**, 614–618.

790 Creech J. B. and Moynier F. (2019) Tin and zinc stable isotope characterisation of chondrites
791 and implications for early Solar System evolution. *Chem. Geol.* **511**, 81–90.
792 Dauphas N. (2017) The isotopic nature of the Earth's accreting material through time. *Nature*
793 **541**, 521–524.
794 Dauphas N., Poitrasson F., Burkhardt C., Kobayashi H. and Kurosawa K. (2015) Planetary and
795 meteoritic Mg/Si and δ30Si variations inherited from solar nebula chemistry. *Earth Planet.*
796 *Sci. Lett.* **427**, 236–248.
797 Davis A. M. (2006) Volatile Evolution and Loss. In *Meteorites and the Early Solar System II* (eds.
798 D. S. Lauretta and H. Y. McSween Jr.). University of Arizona Press. pp. 295–307.
799 Davis A. M. and Richter F. M. (2013) Condensation and Evaporation of Solar System Materials.
800 In *Treatise on Geochemistry: Second Edition* (eds. H. D. Holland and K. K. Turekian). Elsevier
801 Inc. pp. 335–360.
802 Devillers C., Lecomte T. and Hagemann R. (1983) Absolute isotope abundances of tin. *Int. J.*
803 *Mass Spectrom. Ion Phys.* **50**, 205–217.
804 Dodd R. T. (1969) Metamorphism of the ordinary chondrites: A review. *Geochim. Cosmochim.*
805 *Acta* **33**, 161–203.
806 Doucet L. S., Mattielli N., Ionov D. A., Debouge W. and Golovin A. V. (2016) Zn isotopic
807 heterogeneity in the mantle: A melting control? *Earth Planet. Sci. Lett.* **451**, 232–240.
808 Douglas A. E., Howe L. L. and Morton J. R. (1961) The spectrum of the SnS molecule. *J. Mol.*
809 *Spectrosc.* **7**, 161–193.
810 Ducher M., Blanchard M. and Balan E. (2016) Equilibrium zinc isotope fractionation in Zn-
811 bearing minerals from first-principles calculations. *Chem. Geol.* **443**, 87–96.
812 Ebel D. S. (2000). Variations on solar condensation: Sources of interstellar dust nuclei. *Journal of*
813 *Geophysical Research: Space Physics* **105**(A5), 10363-10370.
814 Ebihara M., Wolf R. and Anders E. (1982) Are C1 chondrites chemically fractionated? a trace
815 element study. *Geochim. Cosmochim. Acta* **46**, 1849–1861.
816 Fedkin A. V., Grossman L. and Ghiorso M. S. (2006) Vapor pressures and evaporation
817 coefficients for melts of ferromagnesian chondrule-like compositions. *Geochim.*
818 *Cosmochim. Acta* **70**, 206–223.
819 Fehr M. A., Hammond S. J. and Parkinson I. J. (2018) Tellurium stable isotope fractionation in
820 chondritic meteorites and some terrestrial samples. *Geochim. Cosmochim. Acta* **222**, 17–
821 33.

822 Fehr M. A., Rehkamper M., Halliday A. N., Wiechert U., Hattendorf B., Gunther D., Ono S.,
823 Eigenbrode J. L. and Rumble D. (2005) Tellurium isotopic composition of the early solar
824 system - A search for effects resulting from stellar nucleosynthesis, Sn-126 decay, and
825 mass-independent fractionation. *Geochim. Cosmochim. Acta* **69**, 5099–5112.
826 Fischer R. A., Nakajima Y., Campbell A. J., Frost D. J., Harries D., Langenhorst F., Miyajima N.,
827 Pollok K. and Rubie D. C. (2015) High pressure metal-silicate partitioning of Ni, Co, V, Cr, Si,
828 and O. *Geochim. Cosmochim. Acta* **167**, 177–194.
829 Fitoussi C., Bourdon B. and Wang X. (2016) The building blocks of Earth and Mars: A close
830 genetic link. *Earth Planet. Sci. Lett.* **434**, 151–160.
831 Friedrich J. M., Bridges J. C., Wang M. S. and Lipschutz M. E. (2004) Chemical studies of L
832 chondrites. VI: Variations with petrographic type and shock-loading among equilibrated
833 falls. *Geochim. Cosmochim. Acta* **68**, 2889–2904.
834 Friedrich J. M., Perrotta G. C. and Kimura M. (2014) Compositions, geochemistry, and shock
835 histories of recrystallized LL chondrites. *Geochim. Cosmochim. Acta* **139**, 83–97.
836 Friedrich J. M., Wang M.-S. and Lipschutz M. (2002) Comparison of the trace element
837 composition of Tagish Lake with other primitive carbonaceous chondrites. *Meteorit. Planet.*
838 *Sci.* **37**, 677–686.
839 Friedrich J. M., Wang M.-S. and Lipschutz M. E. (2003) Chemical studies of L chondrites. V:
840 compositional patterns for 49 trace elements in 14 L4-6 and 7 LL4-6 falls. *Geochim.*
841 *Cosmochim. Acta* **67**, 2467–2479.
842 Grossman L., Beckett J. R., Fedkin A. V., Simon S. B. and Ciesla F. J. (2008) Redox conditions in
843 the solar nebula: Observational, experimental, and theoretical constraints. In *Oxygen in*
844 *the Solar System* De Gruyter Mouton. pp. 93–140.
845 Grossman L. and Larimer J. W. (1974) Early chemical history of the solar system. *Rev. Geophys.*
846 **12**, 71–101.
847 Halliday A. N. and Porcelli D. (2001) In search of lost planets - The paleocosmochemistry of the
848 inner solar system. *Earth Planet. Sci. Lett.* **192**, 545–559.
849 Hamaguchi H., Onuma N., Hirao Y., Yokoyama H., Bando S. and Furukawa M. (1969) The
850 abundances of arsenic, tin and antimony in chondritic meteorites. *Geochim. Cosmochim.*
851 *Acta* **33**, 507–518.
852 Hellmann J. L., Hopp T., Burkhardt C., Kleine T. (2020) Origin of volatile element depletion
853 among carbonaceous chondrites. *Earth Planet. Sci. Lett.* **549**, 116508.

Hin R., Coath C., Carter P., Nimmo F., Lai Y.-J., Pogge von Strandmann P. A. E., Willbold M., Leinhardt Z. M., Walter M. J. and Elliott T. (2017) Magnesium isotope evidence that accretional vapour loss shapes planetary compositions. *Nature* **549**, 511–515.

Humayun M. and Cassen P. (2000) Processes Determining the Volatile Abundances of the Meteorites and Terrestrial Planets. *Orig. Earth Moon* **1**, 3–23.

Humayun M. and Clayton R. N. (1995) Potassium isotope cosmochemistry: Genetic implications of volatile element depletion. *Geochim. Cosmochim. Acta* **59**, 2131–2148.

Huss G. R., Rubin A. E. and Grossman J. N. (2006) Thermal Metamorphism in Chondrites. In *Meteorites and the Early Solar System II* p. 567.

Ikramuddin M., Binz C. M. and Lipschutz M. E. (1977) Thermal metamorphism of primitive meteorites-III. Ten trace elements in Krymka L3 chondrite heated at 400-1000°C. *Geochim. Cosmochim. Acta* **41**, 393–401.

Jochum K. P., Hofmann A. W. and Seufert H. M. (1993) Tin in mantle-derived rocks: Constraints on Earth evolution. *Geochim. Cosmochim. Acta* **57**, 3585–3595.

Labidi J., König S., Kurzawa T., Yierpan A. and Schoenberg R. (2018) The selenium isotopic variations in chondrites are mass-dependent; Implications for sulfide formation in the early solar system. *Earth Planet. Sci. Lett.* **481**, 212–222.

De Laeter J. R. and Jeffery P. M. (1965) The isotopic composition of Terrestrial and Meteoritic tin. *J. Geophisical Res.* **70**, 2895–2903.

De Laeter J. R. and Jeffery P. M. (1967) Tin: its isotopic and elemental abundance. *Geochim. Cosmochim. Acta* **31**, 969–985.

De Laeter J. R., McCulloch M. T. and Rosman K. J. R. (1974) Mass Spectrometric Isotope Dilution Analyses of Tin in Stony Meteorites and Standard Rocks. *Earth Planet. Sci. Lett.* **22**, 226–232.

Larimer J. W. (1973) Chemical fractionations in meteorites-VII. Cosmothermometry and cosmobarometry. *Geochim. Cosmochim. Acta* **37**, 1603–1623.

Larimer J. W. and Anders E. (1967) Chemical fractionations in meteorites—II. Abundance patterns and their interpretation. *Geochim. Cosmochim. Acta* **31**, 1239–1270.

Lodders K. (2003) Solar System Abundances and Condensation Temperatures of the Elements. *Astrophys. J.* **591**, 1220–1247.

Lodders K., Palme H. and Gail H.-P. (2009) *4.4 Abundances of the elements in the Solar System*.,

Loss R. D., Rosman K. J. R. and De Laeter J. R. (1990) The isotopic composition of zinc, palladium,

886 silver, cadmium, tin and tellurium in acid-etched residues of the Allende meteorite.
887 *Geochim. Cosmochim. Acta* **54**, 3525–3536.
888 Luck J. M., Othman D. Ben and Albarède F. (2005) Zn and Cu isotopic variations in chondrites
889 and iron meteorites: Early solar nebula reservoirs and parent-body processes. *Geochim.*
890 *Cosmochim. Acta* **69**, 5351–5363.
891 Luck J. M., Othman D. Ben B., Barrat J. A. and Albarède F. (2003) Coupled 63Cu and 16O
892 excesses in chondrites. *Geochim. Cosmochim. Acta* **67**, 143–151.
893 Ma C. and Beckett J. R. (2018) Nuwaite (Ni 6 GeS 2 ) and butianite (Ni 6 SnS 2 ), two new
894 minerals from the Allende meteorite: Alteration products in the early solar system. *Am.*
895 *Mineral.* **103**, 1918–1924.
896 Mahan B., Moynier F., Beck P., Pringle E. A. and Siebert J. (2018a) A history of violence: Insights
897 into post-accretionary heating in carbonaceous chondrites from volatile element
898 abundances, Zn isotopes and water contents. *Geochim. Cosmochim. Acta* **220**, 19–35.
899 Mahan B., Moynier F., Siebert J., Gueguen B., Agranier A., Pringle E. A., Bollard J., Connelly J. N.
900 and Bizzarro M. (2018b) Volatile element evolution of chondrules through time. *Proc. Natl.*
901 *Acad. Sci. U. S. A.* **115**, 8547–8552.
902 Mason B. and Graham A. L. (1970) Minor and trace elements in meteoritic minerals.
903 *Smithsonian Contributions to the Earth Sciences*. 1–17.
904 McNaughton N. J. and Rosman K. J. R. (1991) Tin isotope fractionation in terrestrial cassiterites.
905 *Geochim. Cosmochim. Acta* **55**, 499–504.
906 McSween H. Y. and Labotka T. C. (1993) Oxidation during metamorphism of the ordinary
907 chondrites. *Geochim. Cosmochim. Acta* **57**, 1105–1114.
908 McVay I. R., Maher W. A., Krikowa F. and Ubrhien R. (2019) Metal concentrations in waters,
909 sediments and biota of the far south-east coast of New South Wales, Australia, with an
910 emphasis on Sn, Cu and Zn used as marine antifoulant agents. *Environ. Geochem. Health*
911 **41**, 1351–1367.
912 Morgan J. W., Janssens M. J., Takahashi H., Hertogen J. and Anders E. (1985) H-chondrites:
913 Trace element clues to their origin. *Geochim. Cosmochim. Acta* **49**, 247–259.
914 Moynier F., Fujii T., Telouk P. (2009) Mass-independent isotopic fractionation of tin in chemical
915 exchange reaction using a crown ether. *Analytica Chimica Acta* **632**(2), 234-239.
916 Nebel O., Mezger K. and van Westrenen W. (2011) Rubidium isotopes in primitive chondrites:
917 Constraints on Earth's volatile element depletion and lead isotope evolution. *Earth Planet.*

*Sci. Lett.* **305**, 309–316.

O'Neill H. S. C. (1991) The origin of the moon and the early history of the earth-A chemical model. Part 2: The earth. *Geochim. Cosmochim. Acta* **55**, 1159–1172.

Ozawa K. and Nagahara H. (2001) Chemical and isotopic fractionations by evaporation and their cosmochemical implications. *Geochim. Cosmochim. Acta* **65**, 2171–2199.

Palme H. (2001) Chemical and isotopic heterogeneity in protosolar matter eds. R. Hutchison, C. Pillinger, G. Turner, and S. Russell. *Philos. Trans. R. Soc. London. Ser. A Math. Phys. Eng. Sci.* **359**, 2061–2075.

Palme H. and Hutchison R. (2001) Chemical and isotopic heterogeneity in protosolar matter. *Philos. Trans. R. Soc. A Math. Phys. Eng. Sci.* **359**, 2061–2075.

Palme H. and O'Neill H. (2013) Cosmochemical Estimates of Mantle Composition. In *Treatise on Geochemistry: Second Edition* Elsevier Inc. pp. 1–39.

Pignatale F. C., Gonzalez J.-F., Bourdon B. and Fitoussi C. (2019) Size and density sorting of dust grains in SPH simulations of protoplanetary discs – II. Fragmentation. *Mon. Not. R. Astron. Soc.* **490**, 4428–4446.

Polyakov V. B., Mineev S. D., Clayton R. N., Hu G. and Mineev K. S. (2005) Determination of tin equilibrium isotope fractionation factors from synchrotron radiation experiments. *Geochim. Cosmochim. Acta* **69**, 5531–5536.

Pringle E. A. and Moynier F. (2017) Rubidium isotopic composition of the Earth, meteorites, and the Moon: Evidence for the origin of volatile loss during planetary accretion. *Earth Planet. Sci. Lett.* **473**, 62–70.

Pringle E. A., Moynier F., Beck P., Paniello R. and Hezel D. C. (2017) The origin of volatile element depletion in early solar system material: Clues from Zn isotopes in chondrules. *Earth Planet. Sci. Lett.* **468**, 62–71.

Pringle E. A., Moynier F., Savage P. S., Badro J. and Barrat J. A. (2014) Silicon isotopes in angrites and volatile loss in planetesimals. *Proc. Natl. Acad. Sci. U. S. A.* **111**, 17029–17032.

Righter K. and Drake M. J. (2000) Metal/silicate equilibrium in the early earth-new constraints from the volatile moderately siderophile elements Ga, Cu, P, and Sn. *Geochim. Cosmochim. Acta* **64**, 3581–3597.

Righter K. (2011) Prediction of metal–silicate partition coefficients for siderophile elements: An update and assessment of PT conditions for metal–silicate equilibrium during accretion of the Earth, Earth Planet. Sci. Lett. 304, 158-16.

950 Righter K., Nickodem K., Pando K., Danielson L., Boujibar A., Righter M. and Lapen T. J. (2017)
951 Distribution of Sb, As, Ge, and In between metal and silicate during accretion and core
952 formation in the Earth. *Geochim. Cosmochim. Acta* **198**, 1–16.
953 Righter K., Pando K. M., Danielson L. and Lee C. T. (2010) Partitioning of Mo, P and other
954 siderophile elements (Cu, Ga, Sn, Ni, Co, Cr, Mn, V, and W) between metal and silicate
955 melt as a function of temperature and silicate melt composition. *Earth Planet. Sci. Lett.*
956 **291**, 1–9.
957 Righter K., Pando K., Marin N., Ross D. K., Righter M., Danielson L., Lapen T. J. and Lee C. (2018)
958 Volatile element signatures in the mantles of Earth, Moon, and Mars: Core formation
959 fingerprints from Bi, Cd, In, and Sn. *Meteorit. Planet. Sci.* **53**, 284–305.
960 Rosman K. J. R., Loss R. D. and De Laeter J. R. (1984) The Isotopic composition of Tin. *Int. J. Mass*
961 *Spectrom. Ion Process.* **56**, 281–291.
962 Rosman K. J. R. and Mcnaughton N. J. (1987) High-Precision Measurement of Isotopic
963 Fractionation in Tin. *Int. J. Mass Spectrom. Ion Process.* **75**, 91–98.
964 Rubin A. E. (2005) Relationships among intrinsic properties of ordinary chondrites: Oxidation
965 state, bulk chemistry, oxygen-isotopic composition, petrologic type, and chondrule size.
966 *Geochim. Cosmochim. Acta* **69**, 4907–4918.
967 Rudge J. F., Reynolds B. C. and Bourdon B. (2009) The double spike toolbox. *Chem. Geol.* **265**,
968 420–431.
969 Schaefer L. and Fegley B. (2010) Volatile element chemistry during metamorphism of ordinary
970 chondritic material and some of its implications for the composition of asteroids. *Icarus*
971 **205**, 483–496.
972 Schönbächler M., Carlson R. W., Horan M. F., Mock T. D. and Hauri E. H. (2010) Heterogeneous
973 accretion and the moderately volatile element budget of earth. *Science (80-. ).* **328**, 884–
974 887.
975 Schönbächler M., Carlson R. W., Horan M. F., Mock T. D. and Hauri E. H. (2008) Silver isotope
976 variations in chondrites: Volatile depletion and the initial $^{107}$Pd abundance of the solar
977 system. *Geochim. Cosmochim. Acta* **72**, 5330–5341.
978 Sharp Z. D., Mercer J. A., Jones R. H., Brearley A. J., Selverstone J., Bekker A. and Stachel T.
979 (2013) The chlorine isotope composition of chondrites and Earth. *Geochim. Cosmochim.*
980 *Acta* **107**, 189–204.
981 Shima M. (1964) The distribution of germanium and tin in meteorites. *Geochim. Cosmochim.*

982 *Acta* **28**, 517–532.
983 Siebert J., Corgne A. and Ryerson F. J. (2011) Systematics of metal-silicate partitioning for many
984 siderophile elements applied to Earth's core formation. *Geochim. Cosmochim. Acta* **75**,
985 1451–1489.
986 Sossi P. A., Nebel O., O'Neill H. S. C. and Moynier F. (2018) Zinc isotope composition of the
987 Earth and its behaviour during planetary accretion. *Chem. Geol.* **477**, 73–84.
988 Sugiura N., Brar N. S., Strangway D. W. and Matsui T. (1984) Degassing of meteorite parent
989 body. *J. Geophys. Res.* **89 Suppl**, 641–644.
990 Trinquier A., Birck J. and Allegre C. J. (2007) Widespread 54 Cr Heterogeneity in the Inner Solar
991 System . *Astrophys. J.* **655**, 1179–1185.
992 Vollstaedt H., Mezger K. and Leya I. (2016) The isotope composition of selenium in chondrites
993 constrains the depletion mechanism of volatile elements in solar system materials. *Earth*
994 *Planet. Sci. Lett.* **450**, 372–380.
995 Wai C. M. and Wasson J. T. (1977) Nebular condensation of moderately volatile elements and
996 their abundances in ordinary chondrites. *Earth Planet. Sci. Lett.* **36**, 1–13.
997 Wang D., Mathur R., Powell W., Godfrey L. and Zheng Y. (2019) Experimental evidence for
998 fractionation of tin chlorides by redox and vapor mechanisms. *Geochim. Cosmochim. Acta*
999 **250**, 209–218.
1000 Wang K. and Jacobsen S. B. (2016) Potassium Isotopic Evidence for the Origin of the Moon.
1001 *Submitt. to Nat.*, 1–10.
1002 Wang X., Amet Q., Fitoussi C. and Bourdon B. (2018) Tin isotope fractionation during magmatic
1003 processes and the isotope composition of the bulk silicate Earth. *Geochim. Cosmochim.*
1004 *Acta* **228**, 320–335.
1005 Wang X., Fitoussi C., Bourdon B. and Amet Q. (2017) A new method of Sn purification and
1006 isotopic determination with a double-spike technique for geological and cosmochemical
1007 samples. *J. Anal. At. Spectrom.* **32**.
1008 Wanke H. and Dreibus G. (1988) Chemical Composition and Accretion History of Terrestrial
1009 Planets. *Philos. Trans. R. Soc. London. Ser. A, Math. Phys. Sci.* **325**, 545–557.
1010 Wasson J. T. (1972) Formation of ordinary chondrites. *Rev. Geophys.* **10**, 711–759.
1011 Wasson J. T. and Chou C.-L. (1974) Fractionation of moderately volatile elements in ordinary
1012 chondrites. *Meteoritics* **9**, 69–84.
1013 Wasson J. T. and Kallemeyn G. W. (1988) Compositions of Chondrites. *Philos. Trans. R. Soc. A*

1014 *Math. Phys. Eng. Sci.* **325**, 535–544.
1015 Witt-Eickschen G., Palme H., O'Neill H. S. C. and Allen C. M. (2009) The geochemistry of the
1016 volatile trace elements As, Cd, Ga, In and Sn in the Earth's mantle: New evidence from in
1017 situ analyses of mantle xenoliths. *Geochim. Cosmochim. Acta* **73**, 1755–1778.
1018 Wolf R., Richter G. R., Woodrow A. B. and Anders E. (1980) Chemical fractionations in
1019 meteorites-XI. C2 chondrites. *Geochim. Cosmochim. Acta* **44**, 711–717.
1020 Wombacher F., Rehkämper M., Mezger K., Bischoff A. and Münker C. (2008) Cadmium stable
1021 isotope cosmochemistry. *Geochim. Cosmochim. Acta* **72**, 646–667.
1022 Wombacher F., Rehkämper M., Mezger K. and Münker C. (2003) Stable isotope compositions of
1023 cadmium in geological materials and meteorites determined by multiple-collector ICPMS.
1024 *Geochim. Cosmochim. Acta* **67**, 4639–4654.
1025 Wood B. J., Smythe D. J. and Harrison T. (2019) The condensation temperatures of the elements:
1026 A reappraisal. *Am. Mineral.* **104**, 844–856.
1027 Yin Q. (2005) From Dust to Planets: The Tale Told by Moderately Volatile Elements. In
1028 *Chondrites and the Protoplanetary Disk* p. 632.
1029 Young E. D. (2000) Assessing the implications of K isotope cosmochemistry for evaporation in
1030 the preplanetary solar nebula. *Earth Planet. Sci. Lett.* **183**, 321–333.
1031 Yu Y., Hewins R. H., Alexander C. M. O. D. and Wang J. (2003) Experimental study of
1032 evaporation and isotopic mass fractionation of potassium in silicate melts. *Geochim.*
1033 *Cosmochim. Acta* **67**, 773–786.
1034

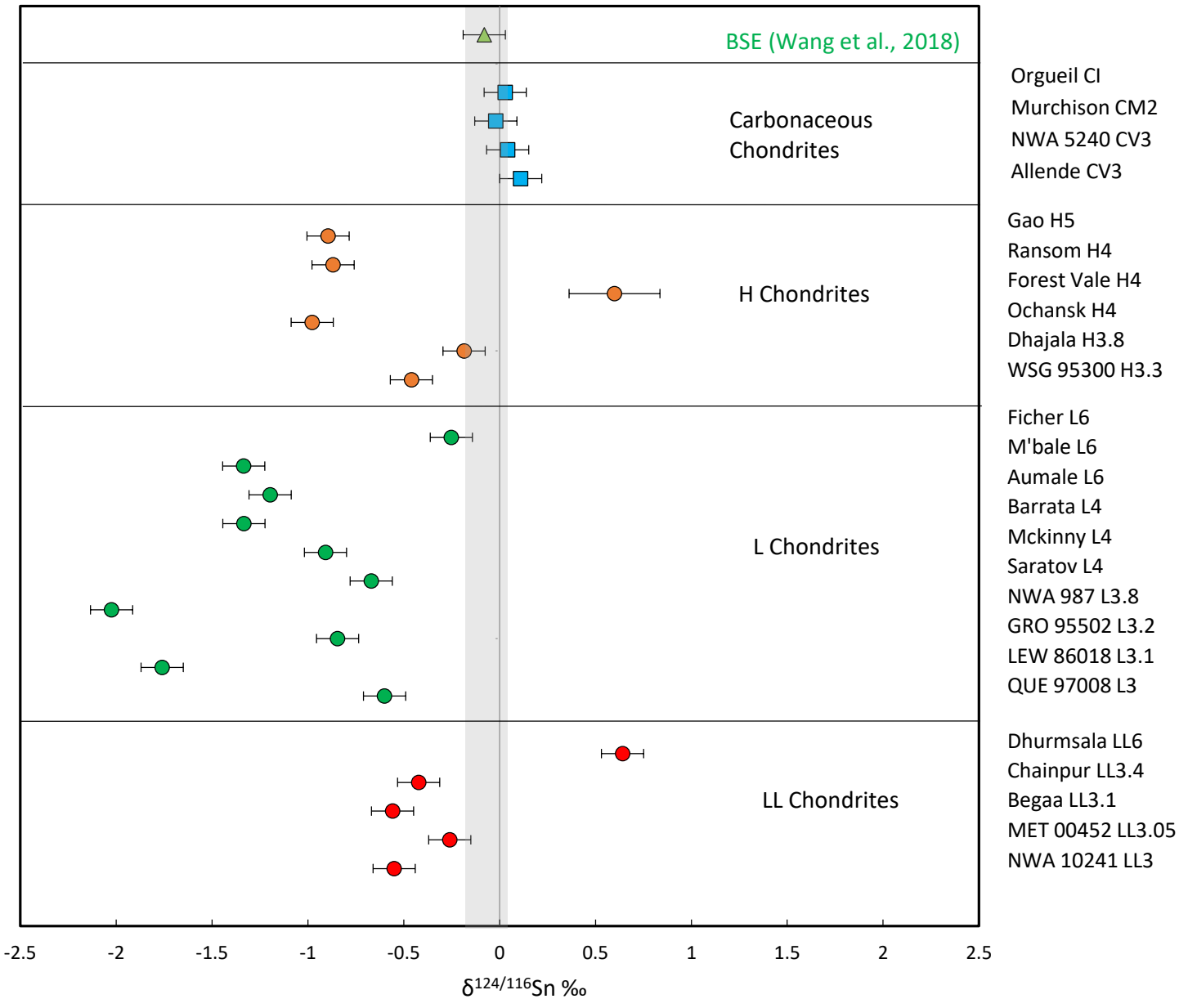
BSE (Wang et al., 2018)
Carbonaceous Chondrites
H Chondrites
L Chondrites
LL Chondrites
Orgueil CI
Murchison CM2
NWA 5240 CV3
Allende CV3
Gao H5
Ransom H4
Forest Vale H4
Ochansk H4
Dhajala H3.8
WSG 95300 H3.3
Ficher L6
M'bale L6
Aumale L6
Barrata L4
Mckinny L4
Saratov L4
NWA 987 L3.8
GRO 95502 L3.2
LEW 86018 L3.1
QUE 97008 L3
Dhurmsala LL6
Chainpur LL3.4
Begaa LL3.1
MET 00452 LL3.05
NWA 10241 LL3
-2.5
-2
-1.5
-1
-0.5
0
0.5
1
1.5
2
2.5
δ124/116Sn ‰

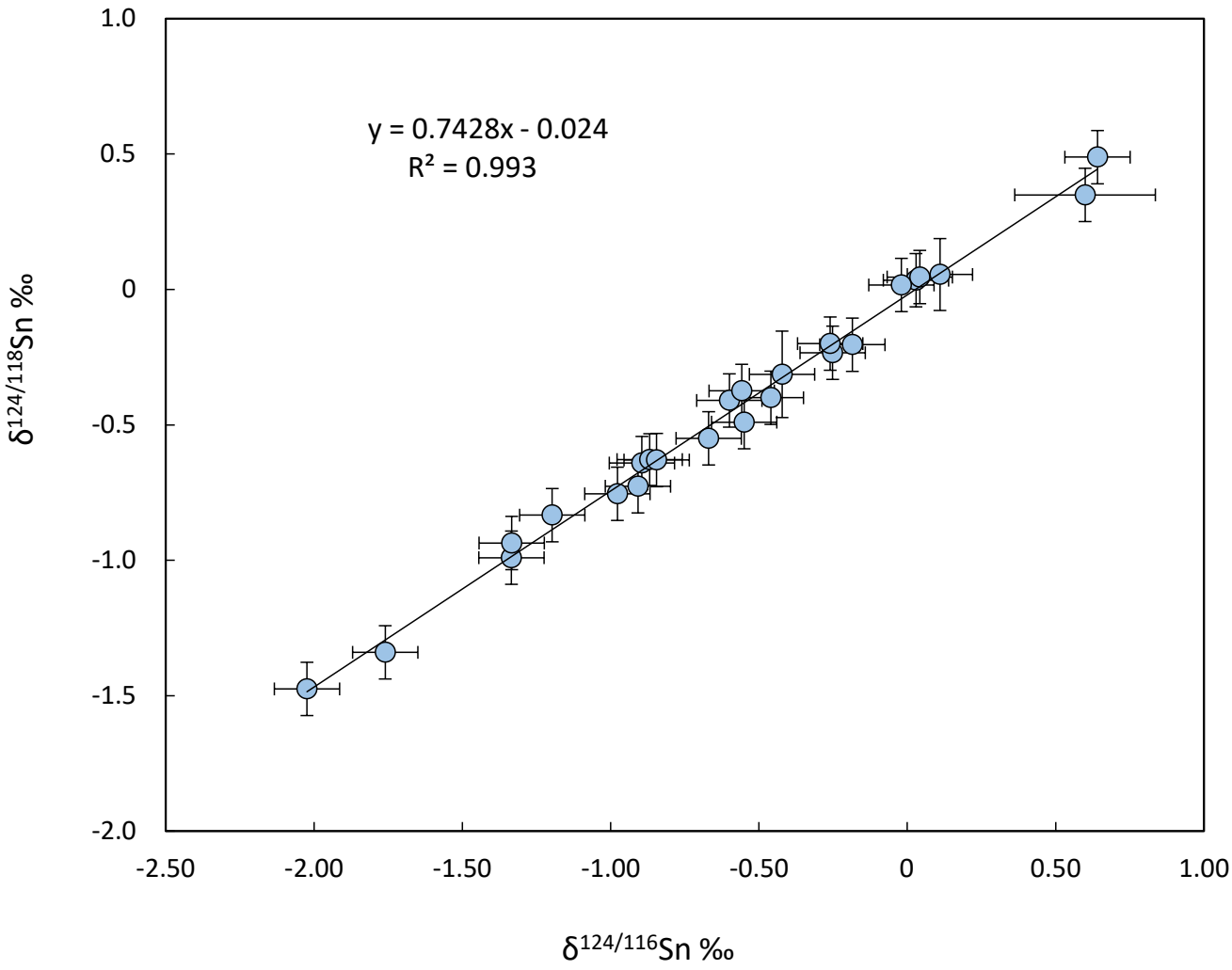
y = 0.7428x - 0.024
R² = 0.993
1.0
0.5
0
-0.5
-1.0
-1.5
-2.0
-2.50
-2.00
-1.50
-1.00
-0.50
0
0.50
1.00
δ124/118Sn ‰
δ124/116Sn ‰

Figure 3

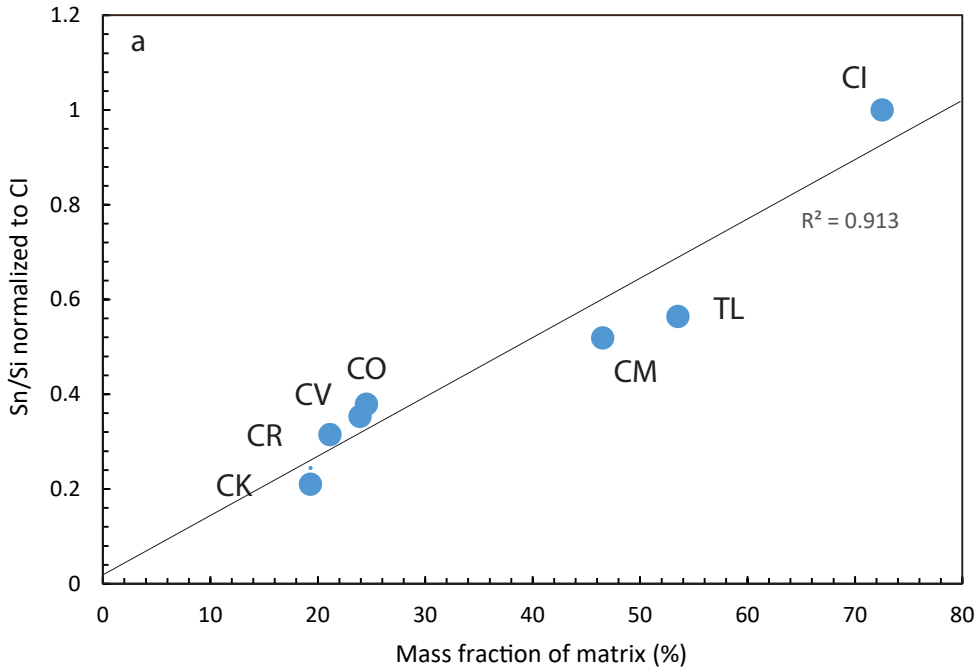
a
Sn/Si normalized to CI
Mass fraction of matrix (%)
R² = 0.913
CI
TL
CM
CO
CV
CR
CK
1.2
1
0.8
0.6
0.4
0.2
0
0
10
20
30
40
50
60
70
80

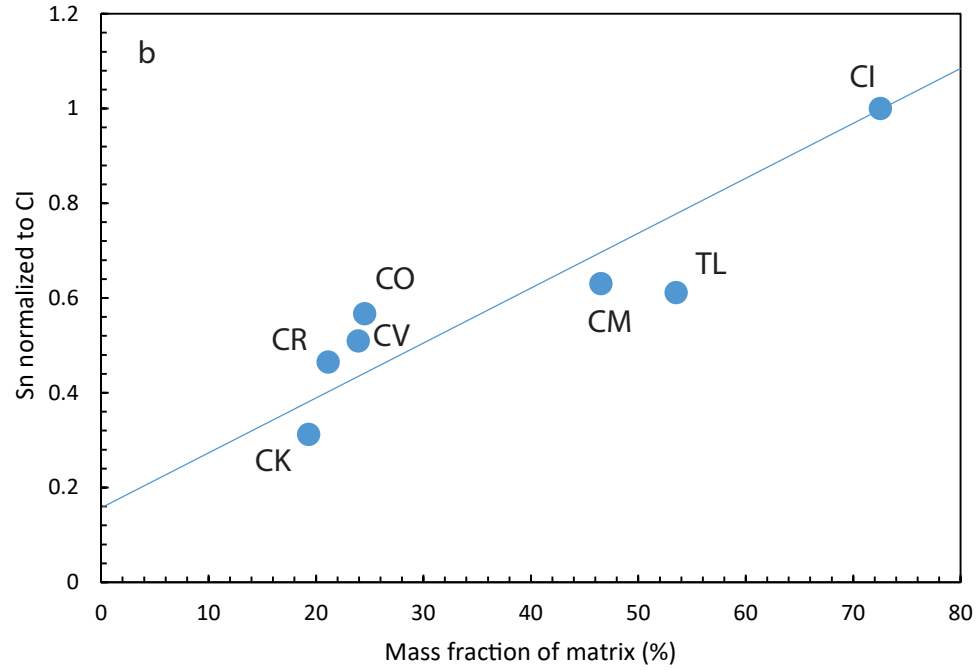
b
Sn normalized to CI
Mass fraction of matrix (%)
CI
TL
CM
CO
CV
CR
CK
1.2
1
0.8
0.6
0.4
0.2
0
0
10
20
30
40
50
60
70
80

Figure 4

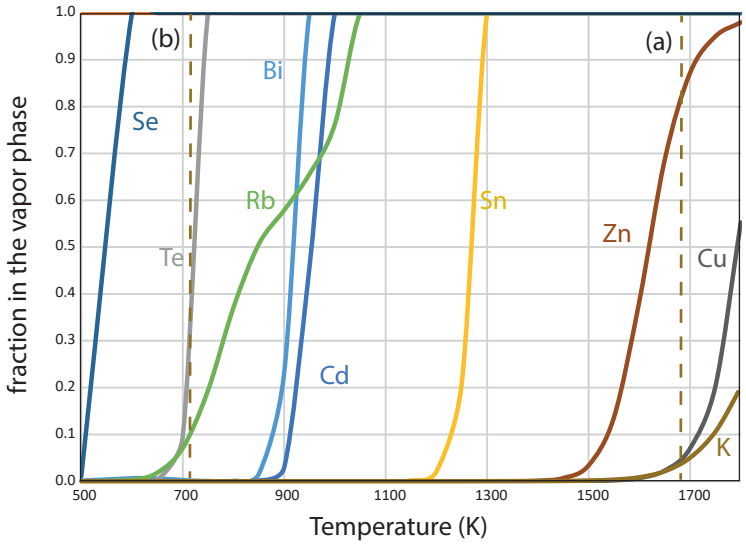
fraction in the vapor phase
1.0
0.9
0.8
0.7
0.6
0.5
0.4
0.3
0.2
0.1
0.0
500
700
900
1100
1300
1500
1700
Temperature (K)
(b)
(a)
Se
Bi
Rb
Te
Cd
Sn
Zn
Cu
K

Figure 5

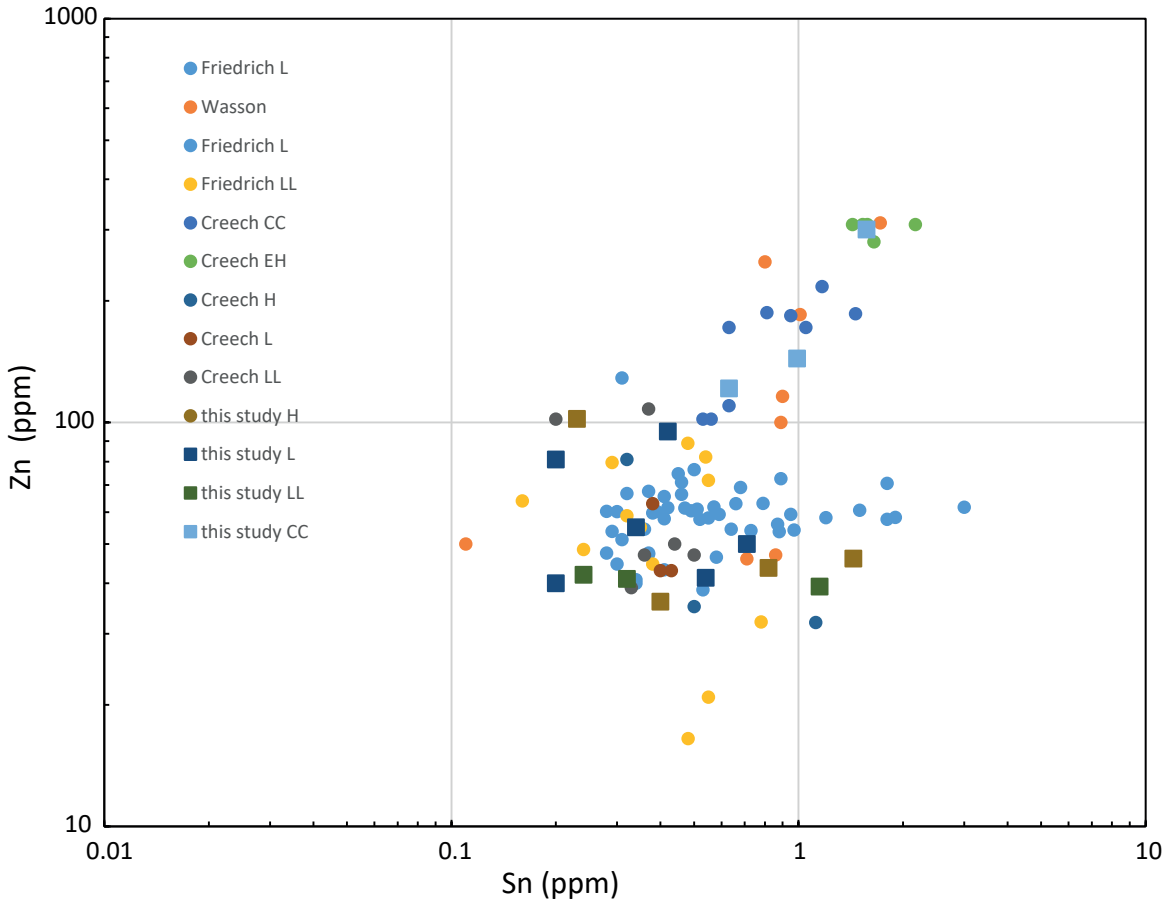
1000
100
10
Zn (ppm)
0.01
0.1
1
10
Sn (ppm)
Friedrich L
Wasson
Friedrich L
Friedrich LL
Creech CC
Creech EH
Creech H
Creech L
Creech LL
this study H
this study L
this study LL
this study CC

Figure 6

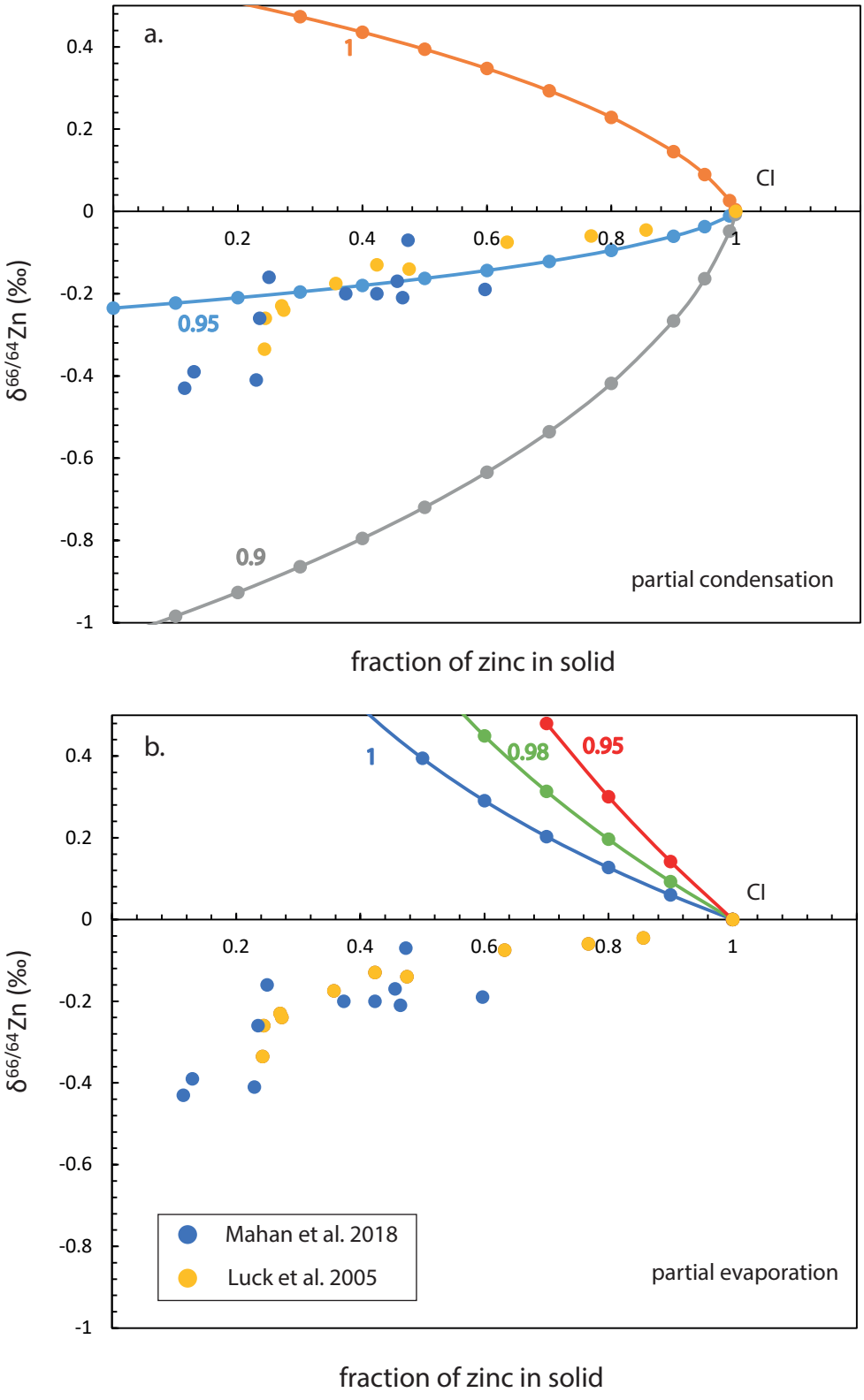
a.
1
CI
0.95
0.9
partial condensation
δ66/64Zn (‰)
fraction of zinc in solid
b.
1
0.98
0.95
CI
Mahan et al. 2018
Luck et al. 2005
partial evaporation
δ66/64Zn (‰)
fraction of zinc in solid

Figure 7

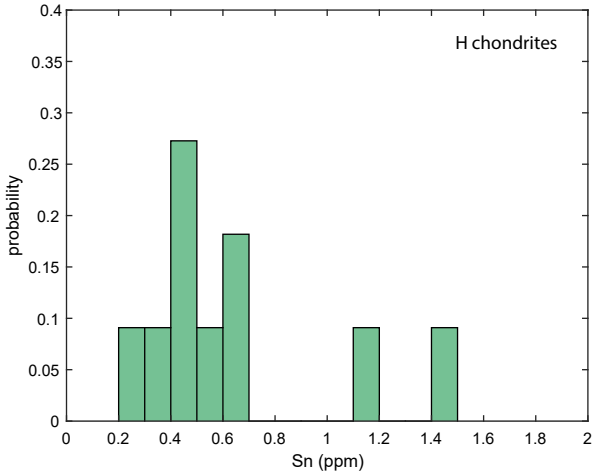
H chondrites
probability
Sn (ppm)
0.4
0.35
0.3
0.25
0.2
0.15
0.1
0.05
0
0 0.2 0.4 0.6 0.8 1 1.2 1.4 1.6 1.8 2

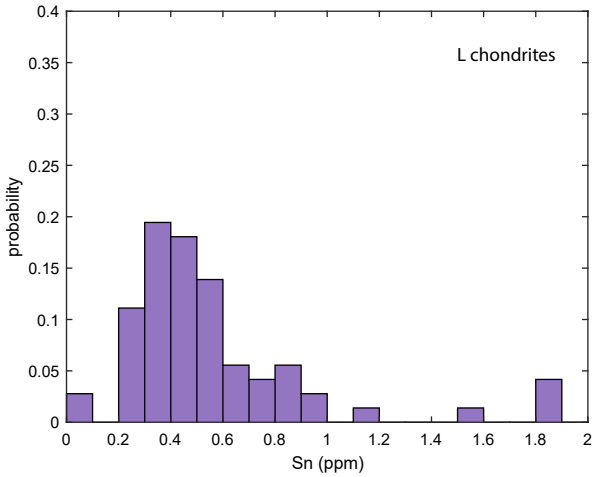
L chondrites
probability
Sn (ppm)
0.4
0.35
0.3
0.25
0.2
0.15
0.1
0.05
0
0 0.2 0.4 0.6 0.8 1 1.2 1.4 1.6 1.8 2

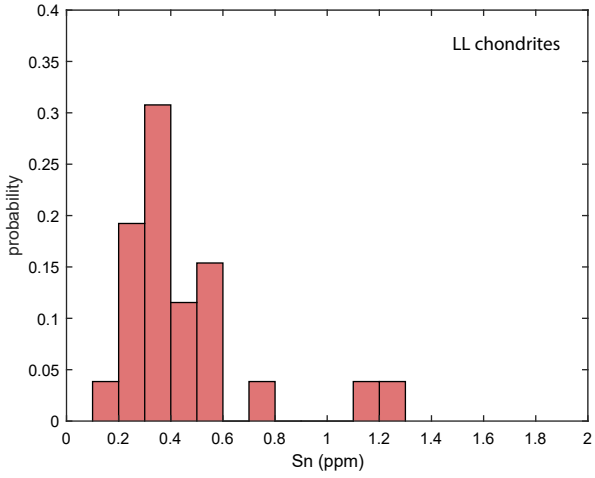
LL chondrites
probability
Sn (ppm)
0.4
0.35
0.3
0.25
0.2
0.15
0.1
0.05
0
0 0.2 0.4 0.6 0.8 1 1.2 1.4 1.6 1.8 2

Figure 8

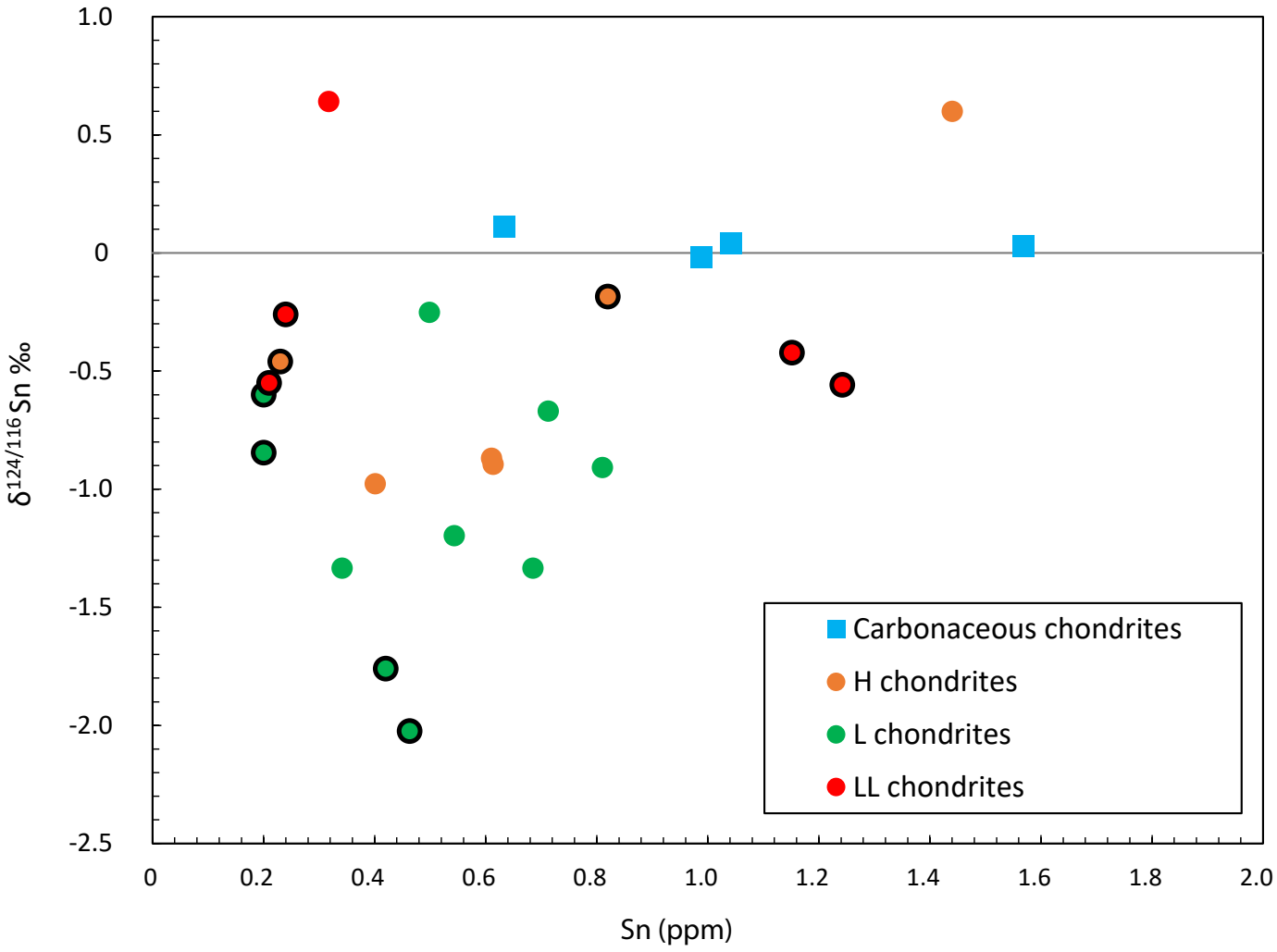
1.0
0.5
0
-0.5
-1.0
-1.5
-2.0
-2.5
δ124/116Sn ‰
0
0.2
0.4
0.6
0.8
1.0
1.2
1.4
1.6
1.8
2.0
Sn (ppm)
Carbonaceous chondrites
H chondrites
L chondrites
LL chondrites

Figure 9

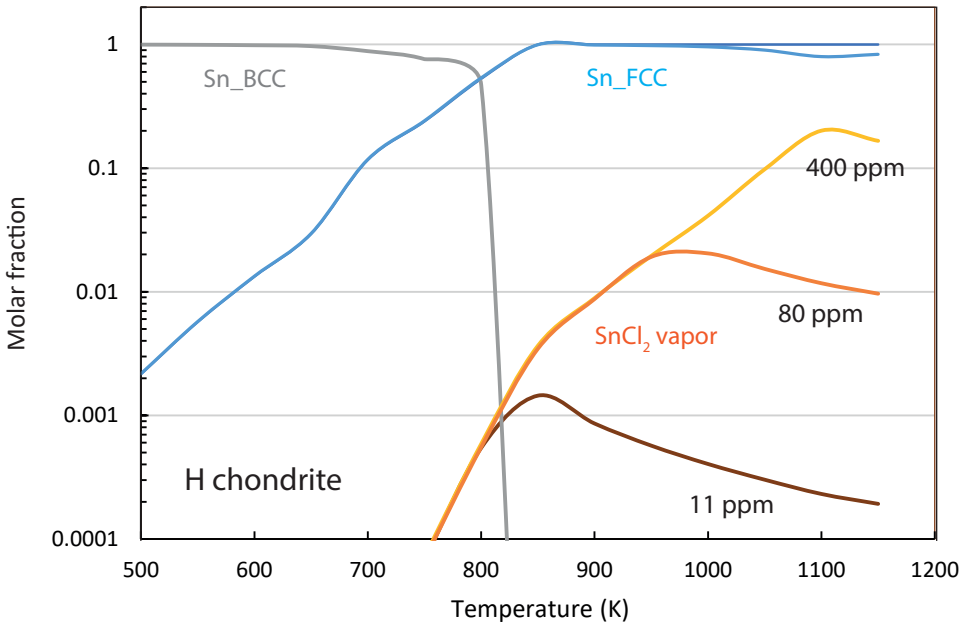
1
0.1
0.01
0.001
0.0001
Molar fraction
Sn_BCC
Sn_FCC
400 ppm
80 ppm
SnCl2 vapor
H chondrite
11 ppm
500
600
700
800
900
1000
1100
1200
Temperature (K)

Figure 10

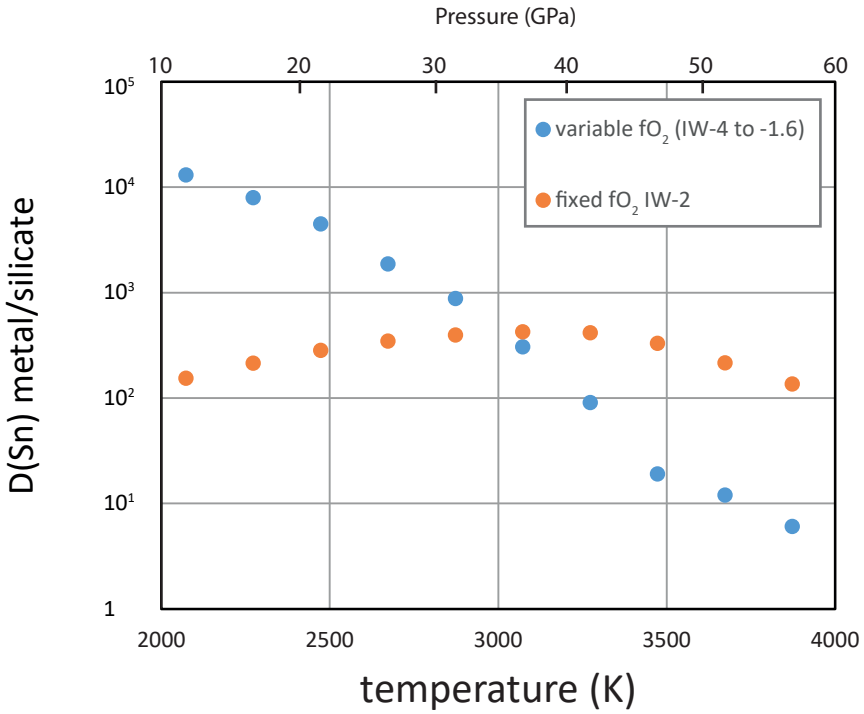
Pressure (GPa)
10
20
30
40
50
60
$10^5$
$10^4$
$10^3$
$10^2$
$10^1$
1
variable $fO_2$ (IW-4 to -1.6)
fixed $fO_2$ IW-2
D(Sn) metal/silicate
2000
2500
3000
3500
4000
temperature (K)

Figure 11

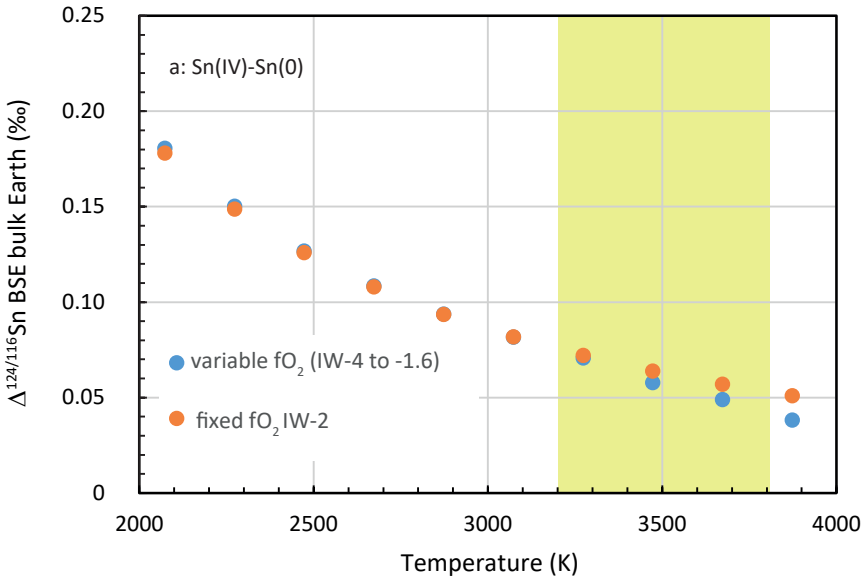
a: Sn(IV)-Sn(0)
variable fO2 (IW-4 to -1.6)
fixed fO2 IW-2
Δ124/116Sn BSE bulk Earth (‰)
Temperature (K)
0.25
0.20
0.15
0.10
0.05
0
2000
2500
3000
3500
4000

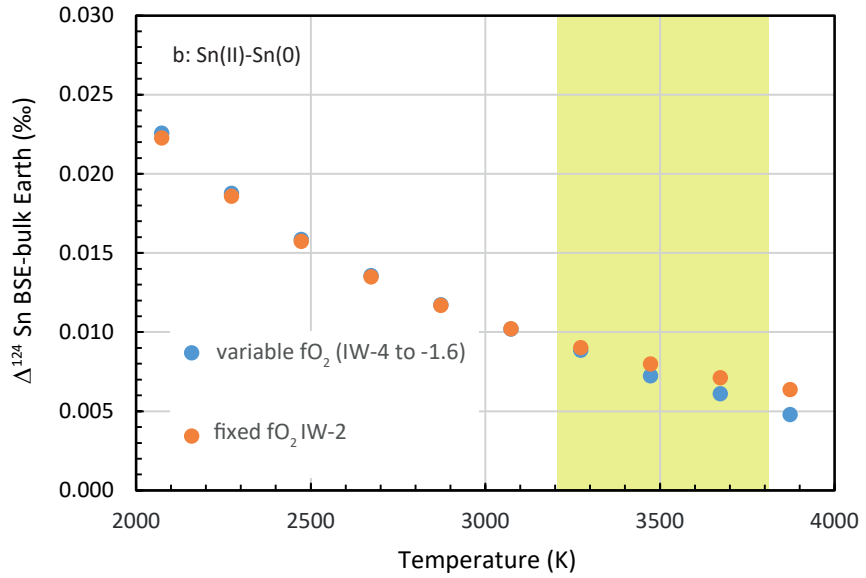
b: Sn(II)-Sn(0)
variable fO2 (IW-4 to -1.6)
fixed fO2 IW-2
Δ124 Sn BSE-bulk Earth (‰)
Temperature (K)
0.030
0.025
0.020
0.015
0.010
0.005
0.000
2000
2500
3000
3500
4000

**Table 1. Sn isotope compositions and concentrations in chondrite samples analyzed in this study.**

| Sample Name | Origin | Shock level | $\delta^{124}$Sn (‰) | 2 s.d. (‰) | $\delta^{124/118}$Sn (‰) | 2 s.d. (‰) | Sn (ppm) | Sample mass (mg) | N* |
|---|---|---|---|---|---|---|---|---|---|
| *Carbonaceous chondrites* | | | | | | | | | |
| Orgueil CI1 | France (fall) | | 0.03 | 0.003 | 0.03 | 0.01 | 1.57±0.13 | 29.1 | 2 |
| Murchison CM2 | Australia (fall) | | -0.02 | 0.05 | 0.02 | 0.05 | 0.99±0.08 | 51.5 | 2 |
| NWA 5240 CV3 | Northwest Africa | | 0.04 | 0.01 | 0.05 | 0.02 | 1.04±0.08 | 59.0 | 2 |
| Allende CV3 | Mexico (fall) | | 0.11 | 0.07 | 0.06 | 0.13 | 0.63±0.01 | 148.4-151.5 | 11 |
| ***Average CC*** | | | **0.04** | **0.11** | | | | | |
| *Ordinary chondrites* | | | | | | | | | |
| Gao-Guenie H5 | Burkina faso (fall) | S1-2 | -0.89 | 0.06 | -0.64 | 0.03 | 0.61±0.05 | 150.5 | 2 |
| Ransom H4 | United States | _ | -0.87 | 0.01 | -0.63 | 0.10 | 0.61±0.05 | 78.2 | 2 |
| Forest Vale H4 | Australia (fall) | S2 | 0.60 | 0.24 | 0.35 | 0.01 | 1.44±0.12 | 57.1 | 2 |
| Ochansk H4 | Russia (fall) | S3 | -0.98 | 0.01 | -0.75 | 0.01 | 0.40±0.03 | 79.5 | 1 |
| Dhajala H3.8 | India (fall) | S1 | -0.19 | 0.02 | -0.20 | 0.02 | 0.82±0.07 | 40.2 | 2 |
| WSG 95300 H3.3 | Antarctica | S2 | -0.46 | 0.05 | -0.40 | 0.05 | 0.23±0.02 | 307.4 | 2 |
| Fisher L6 | United States (fall) | S5 | -0.25 | 0.003 | -0.23 | 0.02 | 0.50±0.04 | 139.8 | 2 |
| Mbale L6 | Uganda | S6 | -1.33 | 0.01 | -0.99 | 0.01 | 0.68±0.05 | 149.6 | 1 |
| Aumale L6 | Algeria (fall) | S2 | -1.20 | 0.02 | -0.83 | 0.04 | 0.54±0.04 | 53.2-68.1 | 2 |
| Barratta L4 | Australia | S4 | -1.33 | 0.01 | -0.94 | 0.01 | 0.34±0.03 | 81.8 | 2 |
| Mckinney L4 | United States | S4-5, S6 | -0.91 | 0.04 | -0.73 | 0.09 | 0.81±0.06 | 74.3 | 2 |
| Saratov L4 | Russia (fall) | S2 | -0.67 | 0.02 | -0.55 | 0.02 | 0.71±0.04 | 75.2 | 4 |
| NWA 987 L3.8 | Northwest Africa | S5 | -2.02 | 0.03 | -1.48 | 0.02 | 0.46±0.04 | 79.3 | 2 |
| GRO 95502 L3.2 | Antarctica | S3 | -0.85 | 0.01 | -0.63 | 0.05 | 0.20±0.03 | 156.8 | 2 |
| LEW 86018 L3.1 | Antarctica | S2 | -1.76 | 0.03 | -1.34 | 0.02 | 0.42±0.03 | 157.2 | 2 |
| QUE 97008 L3.05 | Antarctica | S3 | -0.60 | 0.05 | -0.41 | 0.09 | 0.20±0.03 | 303.2 | 2 |
| Dhurmsala LL6 | India (fall) | S3 | 0.64 | 0.01 | 0.49 | 0.01 | 0.32±0.03 | 78.5 | 1 |
| Chainpur LL3.4 | India (fall) | S1 | -0.42 | 0.04 | -0.31 | 0.16 | 1.15±0.09 | 69.2 | 3 |
| Begaa (NWA 4910) LL3.1 | Northwest Africa | S2 | -0.56 | 0.02 | -0.37 | 0.02 | 1.24±0.10 | 51.1 | 2 |
| MET 00452 LL3.05 | Northwest Africa | _ | -0.26 | 0.02 | -0.20 | 0.003 | 0.24±0.03 | 308.1 | 2 |
| NWA 10241 LL3 | Antarctica | S3 | -0.55 | 0.001 | -0.49 | 0.02 | 0.21±0.02 | 253.0 | 2 |

*The number of replicates N are the sum of measurement replicates. Allende(CV3) and Saratov(L4) have four and two full chemistry replicates, respectively, with three or two measurements for each full replicate. The uncertainties of these two samples are also for full chemistry replicates given as 2 s.d.